Tetraspanin CD53 controls T cell immunity through regulation of CD45RO stability, mobility, and function

Vera-Marie E Dunlock, Abbey B Arp, Simar Pal Singh, Stéphanie Charrin, Viet Nguyen, Erik Jansen, Fleur Schaper, Martin Ter Beest, Malou Zuidscherwoude, Sjoerd J van Deventer, et al.

Cell Reports

Article

Tetraspanin CD53 controls T cell immunity through regulation of CD45RO stability, mobility, and function

Graphical abstract

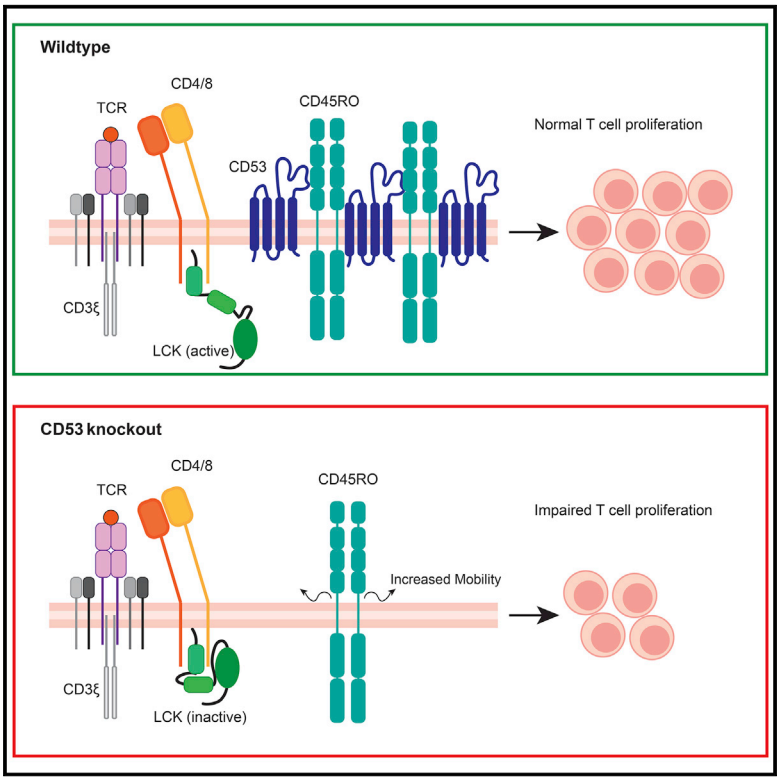

Highlights

- Tetraspanin CD53 interacts with CD45 at the T cell surface
- CD53 is required for CD45RO expression and mobility
- CD53-deficient T cells are impaired in TCR signaling and proliferation
- CD53 is important for T cell-mediated immunity *in vivo*

Authors

Vera-Marie E. Dunlock, Abbey B. Arp, Simar Pal Singh, ..., Laia Querol Cano, Eric Rubinstein, Annemiek B. van Spriel

Correspondence

annemiek.vanspriel@radboudumc.nl

In brief

T cells depend on the phosphatase CD45 to initiate T cell receptor signaling. Dunlock et al. show that tetraspanin CD53 is required for CD45 function, T cell proliferation, and cellular immunity *in vivo*.

Dunlock et al., 2022, Cell Reports *39*, 111006
June 28, 2022
https://doi.org/10.1016/j.celrep.2022.111006

CellPress

Cell Reports

CellPress
OPEN ACCESS

Article

Tetraspanin CD53 controls T cell immunity through regulation of CD45RO stability, mobility, and function

Vera-Marie E. Dunlock,[1] Abbey B. Arp,[1,8] Simar Pal Singh,[1,8] Stéphanie Charrin,[2] Viet Nguyen,[3] Erik Jansen,[1] Fleur Schaper,[1] Martin Ter Beest,[1] Malou Zuidscherwoude,[1] Sjoerd J. van Deventer,[1] Britt Nakken,[4,5] Peter Szodoray,[4,5] Maria C. Demaria,[6] Mark D. Wright,[6] Laia Querol Cano,[1,7] Eric Rubinstein,[2,7] and Annemiek B. van Spriel[1,9,*]

[1]Department of Tumor Immunology, Radboud Institute for Molecular Life Sciences, Radboud University Medical Center, 6525GA Nijmegen, the Netherlands

[2]Sorbonne Université, INSERM, CNRS, Centre d'Immunologie et des Maladies Infectieuses, CIMI-Paris, 75013 Paris, France

[3]Université Paris-Saclay, INSERM, UMS33, 94800 Villejuif, France

[4]Department of Immunology, Oslo University Hospital Rikshospitalet and University of Oslo, NO-0424 Oslo, Norway

[5]K.G. Jebsen Centre for B Cell Malignancies, Institute of Clinical Medicine, University of Oslo, Oslo, Norway

[6]Department of Immunology, Monash University, Alfred Medical Research and Education Precinct, Melbourne, VIC 3004, Australia

[7]These authors contributed equally

[8]These authors contributed equally

[9]Lead contact

*Correspondence: annemiek.vanspriel@radboudumc.nl

https://doi.org/10.1016/j.celrep.2022.111006

SUMMARY

T cells depend on the phosphatase CD45 to initiate T cell receptor signaling. Although the critical role of CD45 in T cells is established, the mechanisms controlling function and localization in the membrane are not well understood. Moreover, the regulation of specific CD45 isoforms in T cell signaling remains unresolved. By using unbiased mass spectrometry, we identify the tetraspanin CD53 as a partner of CD45 and show that CD53 controls CD45 function and T cell activation. CD53-negative T cells (*Cd53*$^{-/-}$) exhibit substantial proliferation defects, and *Cd53*$^{-/-}$ mice show impaired tumor rejection and reduced IFNγ-producing T cells compared with wild-type mice. Investigation into the mechanism reveals that CD53 is required for CD45RO expression and mobility. In addition, CD53 is shown to stabilize CD45 on the membrane and is required for optimal phosphatase activity and subsequent Lck activation. Together, our findings reveal CD53 as a regulator of CD45 activity required for T cell immunity.

INTRODUCTION

T cells are central to the immune responses against pathogens and cancer. T cell responses are initiated at the T cell receptor (TCR), which recognizes antigen presented by major histocompatibility complexes (MHCs). Signaling downstream of the TCR is a requisite for the activation, differentiation, and proliferation, which drives adaptive immunity. Central to this signaling process is the receptor-type protein tyrosine phosphatase CD45 (PTPRC), which occupies ~10% of the T cell surface (Craig et al., 1994; Oka et al., 2000). In the absence of CD45, T cells are incapable of activation (Pingel and Thomas, 1989). The importance of CD45 expression on T cells was highlighted recently by its identification as a biomarker for severe acute respiratory syndrome coronavirus 2 cases (Jin et al., 2020).

CD45 regulates the activity of Src family kinase Lck, the initiator of TCR signaling, by dephosphorylating Lck (at Y505), relieving inhibition and allowing auto-phosphorylation of Y394 (Furlan et al., 2014; Nyakeriga et al., 2012). Activated Lck phosphorylates the CD3 ξ-chains and the downstream kinase ZAP70, initiating TCR signaling. In addition, CD45 can inhibit T cell activation by suppressing ξ-chain phosphorylation, allowing CD45 to adjust the T cell response based on signal strength to prevent disproportionate reactions (Furukawa et al., 1994). This CD45-mediated tuning of TCR signaling has been described by the kinetic segregation (KS) model, which proposes that the tight contacts between immune cells upon TCR engagement can physically separate large glycoproteins, like CD45, from the TCR (Chang et al., 2016). Recent work has revealed that segregation occurs within seconds of TCR engagement and that CD45 distance from the TCR must be tightly controlled for optimal T cell activation (Razvag et al., 2018). Thus, although the KS model identifies an important process during early TCR activation, it cannot explain the complex regulation of CD45 localization and dynamics during TCR signaling, indicating that additional unidentified mechanisms must exist.

The functional importance of CD45 has been demonstrated in CD45-deficient mice, which exhibit severe defects in T cell development and activation, leading to an almost complete absence of peripheral T cells (Byth et al., 1996; Kishihara et al.,

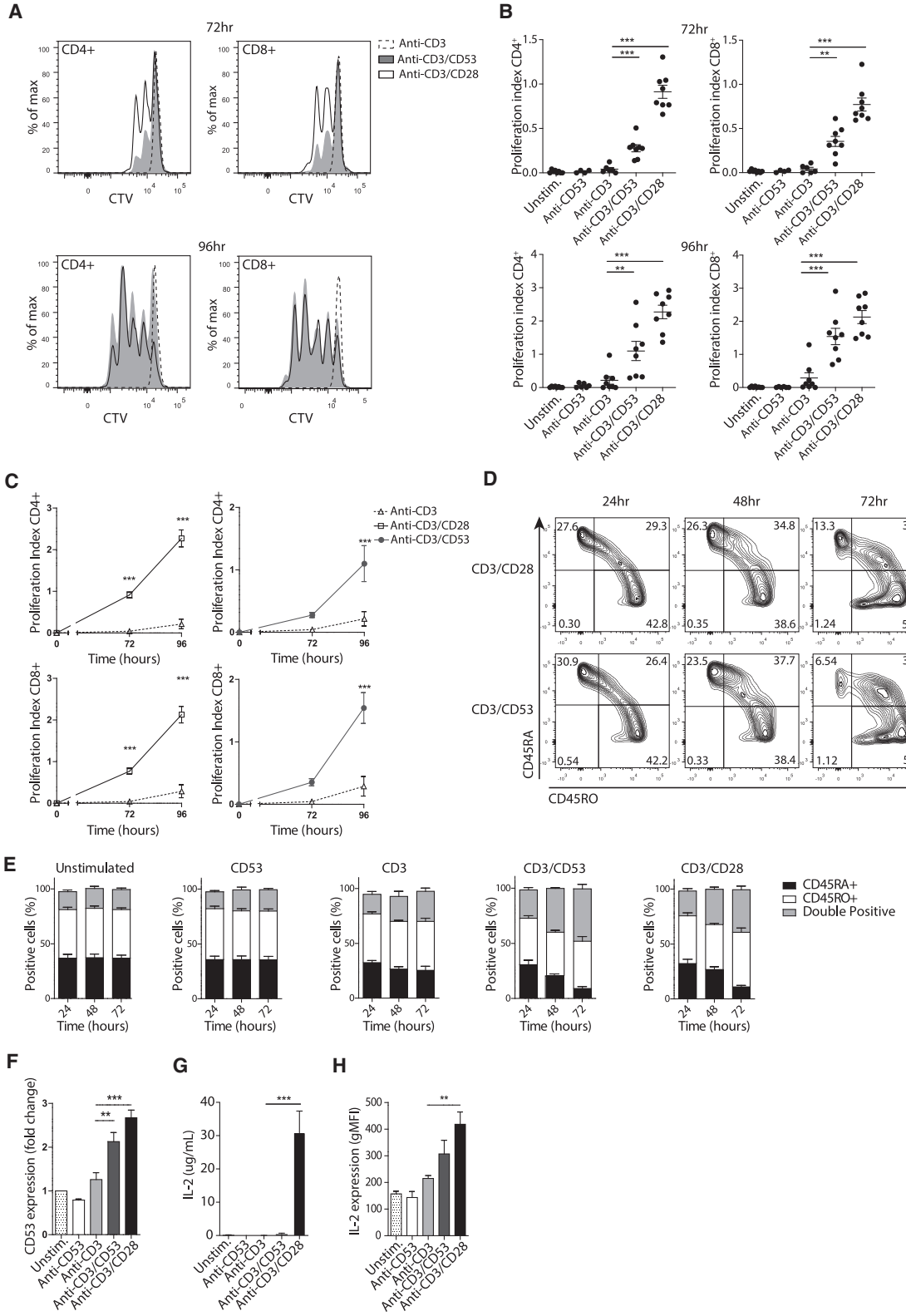

(legend on next page)

1993). In humans, mutations of CD45 have been linked to severe combined immunodeficiency (SCID), autoimmune disorders, and cancer (Porcu et al., 2012; Roberts et al., 2012; Tackenberg et al., 2003).

CD45 is a large transmembrane glycoprotein (180–220 kDa) encoded by 35 exons, producing multiple isoforms through selective inclusion of exons 4, 5, and 6, referred to as A, B, and C, respectively (McNeill et al., 2004). Naive human T cells express mainly high molecular weight (MW) isoforms containing the A exon ($CD45RA^+$ cells). The expression of CD45RA is lost upon activation, resulting in effector/memory T cells expressing the lowest MW isoform CD45RO ($CD45RO^+$ cells), and a similar phenotypic switch has been reported in mice (Birkeland et al., 1989; Clement, 1992). Thus, lower MW isoforms of CD45 are associated with differentiated effector T cell function and memory.

Expression of distinct CD45 isoforms serves an important function in the immune system. Patients carrying mutations resulting in impaired CD45 splicing exhibit an altered T cell phenotype ratio and increased susceptibility to autoimmune and infectious diseases (Tchilian and Beverley, 2006; Tchilian et al., 2001; Vogel et al., 2003). Moreover, genetically altering the combination of isoforms expressed by T cells has been shown to increase the onset and severity of autoimmunity (Dawes et al., 2006). In addition, CD45 isoforms exhibit differential association with CD4/CD8, which affects downstream signal transduction (Dornan et al., 2002).

Here we show that CD45RO stability and function in T cells is specifically regulated by the tetraspanin CD53. Tetraspanins are a family of 4-transmembrane proteins involved in membrane spatial organization. They form tetraspanin nanodomains in the membrane that bring together other tetraspanins and partner proteins to regulate function (Charrin et al., 2014; van Deventer et al., 2021; Levy and Shoham, 2005). Tetraspanins are important for numerous cellular functions, including adhesion and migration, fusion, and cell signaling (Dunlock, 2020; Termini and Gillette, 2017; Yáñez-Mó et al., 2009). We have recently shown that CD53 is important for B cell signaling and the humoral immune response (Demaria et al., 2020; Zuidscherwoude et al., 2017).

In this study, we report a molecular interaction between CD45 and CD53 on the immune cell surface. This interaction was found to regulate the membrane stability and mobility of CD45RO specifically, resulting in an altered CD45 isoform expression pattern upon loss of CD53. Strikingly, T cells lacking CD53 had altered CD45 phosphatase activity, which resulted in defective T cell immunity. Thus, our study reveals an isoform-specific mechanism for the regulation of CD45 at the plasma membrane, which occurs via CD53 and is important for T cell activation *in vivo*.

RESULTS

CD53 modulates the activation of primary human T cells

CD53 function was first investigated in human T cells *in vitro*. Significant proliferation was observed upon stimulation of purified $CD4^+$ and $CD8^+$ T cells with a combination of CD3 and CD53 antibodies (anti-CD3/CD53) in contrast to CD3 or CD53 stimulation alone, indicating that CD53 stimulation induces T cell activation but only when combined with CD3 (Figures 1A–1C).

To establish whether stimulation via anti-CD3/CD53 led to an activated/effector T cell phenotype, we assessed expression of CD45RA (naive) and CD45RO (effector/memory). Stimulation with either anti-CD3/CD28 or anti-CD3/CD53 resulted in an equivalent transition from CD45RA to CD45RO positivity over time (Figures 1D and 1E). This was not observed for unstimulated, or anti-CD3 or anti-CD53 stimulated T cells. We hypothesized that if CD53 is important for T cell activation, expression might be upregulated upon stimulation. Indeed, a significant increase in CD53 surface expression was observed following activation with either anti-CD3/CD53 or anti-CD3/CD28 (Figure 1F).

Next, we assessed whether stimulation via anti-CD3/CD53 was dependent on CD28 co-stimulation. Since high interleukin-2 (IL-2) production is a hallmark CD28 signaling, we measured IL-2 production and secretion. Results show significant amounts of IL-2 were only generated by T cells stimulated via anti-CD3/CD28, not in unstimulated, or anti-CD3, anti-CD53, and anti-CD3/CD53 stimulated T cells (Figure 1G). To exclude the possibility of IL-2 retention, intracellular flow cytometry was performed. T cells stimulated with anti-CD3/CD28 had significant intracellular IL-2 stores, contrary to T cells stimulated with anti-CD3 or anti-CD53 alone. Anti-CD3/CD53 stimulated T cells showed a small increase in intracellular IL-2, although not significant (Figure 1H). These results indicate that T cell activation induced by anti-CD3/CD53 stimulation results in proliferation and transition of primary human T cells toward an effector/memory phenotype via a CD28-independent pathway.

Cd53$^{-/-}$ T cells exhibit an impaired activation response

CD53 is a marker for positively selected $CD4^+$ $CD8^+$ thymocytes (Puls et al., 2002; Tomlinson et al., 1995). Therefore, we

Figure 1. CD53 modulates the activation of primary human T cells

(A) $CD4^+$ and $CD8^+$ T cell proliferation measured by flow cytometry. Graphs are of one representative donor 72 and 96 h post-stimulation. CD3- (dashed line), CD3/CD53- (gray filled), and CD3/CD28- (black line) antibody-stimulated samples are shown.

(B) Proliferation index (PI) of $CD4^+$ and $CD8^+$ T cells 72 and 96 h post-stimulation (n = 8 donors, four independent experiments, mean ± SEM, unpaired two-sided t test).

(C) Changes in PI over time for CD3-, CD3/CD53-, or CD3/CD28-antibody-stimulated T cells (mean ± SEM, two-way ANOVA).

(D) Two-parameter zebra plots depicting T cell expression of CD45RA and CD45RO over time, after stimulation with CD3/CD53- or CD3/CD28-antibodies. Representative data from one donor measured at multiple time points.

(E) Quantification of CD45RA and CD45RO expression over time post-stimulation with indicated antibodies or unstimulated (n = 6 donors from three independent experiments, mean ± SEM).

(F) Expression of CD53 on primary human T cells measured by flow cytometry 72 h post-stimulation with indicated antibodies or unstimulated. Data are fold-change relative to unstimulated samples.

(G and H) IL-2 production by T cells stimulated for 24 h with indicated antibodies or unstimulated by ELISA (G) and intracellular flow cytometry (H). (F–H) n = 6 donors from three independent experiments (mean ± SEM, unpaired two-sided t test). *$p < 0.05$, **$p < 0.01$, ***$p < 0.001$.

investigated whether the absence of CD53 affected T cell development in *Cd53*-deficient (*Cd53*$^{-/-}$) mice. No differences in the percentages of CD4$^+$, CD8$^+$, or double-positive T cell populations were observed in thymi, spleens, and lymph nodes of 6-week-old *Cd53*$^{-/-}$ and wild-type (WT: *Cd53*$^{+/+}$ littermate) mice, or in the percentage of memory or naive T cells in WT and *Cd53*$^{-/-}$ spleen or lymph nodes (Figures S1A and S1B). In line with others, we observed some differences in the number of T cells and total cells localized to primary or secondary immune compartments (Yeung et al., 2020) (Figure S1C). The number of T cells and total cells in the spleen did not differ significantly between WT and *Cd53*$^{-/-}$ mice; however, in the lymph node compartment we did observe significant differences in the size of both the total and T cell population. T cells used in the experiments detailed here were therefore always isolated from spleen unless otherwise stated. Furthermore, similar expression levels and percentages of CD3$^+$, CD4$^+$, CD8$^+$, and CD28$^+$ T cells were found in the spleen and lymph nodes of WT and *Cd53*$^{-/-}$ mice, with the exception of the percentage of CD3$^+$ cells in the lymph node compartment, which was higher in *Cd53*$^{-/-}$ mice due to a known B cell migration deficit (Figure S1D) (Demaria et al., 2020). Taken together, these data indicate that CD53 is not required for normal T cell development in mice.

Next, we investigated whether CD53 deficiency altered T cell proliferation. A striking reduction in proliferation of both CD4$^+$ and CD8$^+$ *Cd53*$^{-/-}$ T cells was observed compared with WT T cells upon anti-CD3/CD28 stimulation (anti-TCR) (Figure 2A). Importantly, no difference in the number of cells entering division between WT and *Cd53*$^{-/-}$ T cells was observed, indicating that the proliferation defect is not caused by a subset of unresponsive *Cd53*$^{-/-}$ T cells, but due to a general proliferation delay in the whole *Cd53*$^{-/-}$ T cell population (Figure 2B). Quantification revealed that *Cd53*$^{-/-}$ T cells undergo significantly less proliferation compared with WT T cells upon anti-TCR stimulation. This was the case for both CD4$^+$ and CD8$^+$ T cell populations, indicating an overall impaired activation in *Cd53*$^{-/-}$ T cells (Figures 2C and 2D).

Further characterization revealed similar expression of the early activation markers CD25 and CD69 on WT and *Cd53*$^{-/-}$ T cells after either phorbol myristate acetate (PMA) or anti-TCR stimulation, confirming that all *Cd53*$^{-/-}$ T cells are responsive to anti-TCR stimulation with no unresponsive subpopulation present (Figure 2E). Furthermore, no differences were seen in IL-2 production by these cells after anti-TCR stimulation, verifying that CD53 function in T cell activation is independent of CD28 (Figure 2F). Overall, these results demonstrate that *Cd53*$^{-/-}$ T cells exhibit impaired proliferation compared with WT cells, which is caused by a defect in *Cd53*$^{-/-}$ T cells.

T cells of *Cd53*$^{-/-}$ mice are impaired in their recall response and tumor rejection capacity

To investigate CD53 function in the recall capacity of T cells post-immunization, we used the model T cell antigen keyhole limpet hemocyanin (KLH) (Figure S1E). In line with our *in vitro* data, *in vivo* primed, antigen-specific, CD4$^+$ T cells from *Cd53*$^{-/-}$ mice, showed diminished proliferation upon restimulation with KLH compared with WT T cells (Figure 3A). Non-immunized mice showed no significant proliferation upon KLH exposure for either genotype, verifying that responses were antigen specific. Quantification confirmed significantly lower proliferation indexes for KLH-specific CD4$^+$ T cells of *Cd53*$^{-/-}$ mice compared with WT mice (Figures 3B and 3C). Moreover, a significantly higher percentage of the total WT CD4$^+$ T population entered division upon KLH restimulation compared with *Cd53*$^{-/-}$ T cells (Figure 3D). These findings show that *in vivo* activation of *Cd53*$^{-/-}$ T cells is impaired, leading to a diminished recall response upon rechallenge.

To further investigate the recall capacity of *Cd53*$^{-/-}$ T cells, *Cd53*$^{-/-}$ and WT mice were immunized with γ-irradiated B16OVA tumor cells and T cells were analyzed for interferon-γ (IFN-γ) production. Significantly fewer IFN-γ-producing CD8$^+$ T cells were detected in the *Cd53*$^{-/-}$ splenocyte population compared with WT upon exposure to the OVA peptide SIINFEKL (Figure 3E). These results confirm defective activation of *Cd53*$^{-/-}$ T cells *in vivo* and demonstrate that this impairs antigen-specific T cell responses.

To exclude that the T cell activation defect was due to impairment of dendritic cells (DCs) in the absence of CD53, we analyzed primary DCs from *Cd53*$^{-/-}$ mice. Similar numbers of DC subsets (plasmacytoid and conventional DCs) were isolated from spleens of *Cd53*$^{-/-}$ and WT mice, and these DCs expressed comparable levels of MHC classes I and II (Figures S2A–S2B). In addition, DC differentiation from bone marrow of WT and *Cd53*$^{-/-}$ mice was similar between both genotypes (Figure S2C). These results indicate that the development and differentiation of *Cd53*$^{-/-}$ DCs is normal. Next, we assessed the antigen-presentation capacity of *Cd53*$^{-/-}$ and WT DCs. We observed no differences in the MHC-I and MHC-II presentation capacity of WT and *Cd53*$^{-/-}$ DCs as measured by OT-II T cell proliferation (Figure S2D) and OTI T cell proliferation *in vivo* (Figure S2E). Together, these data show that the antigen-presentation capacity of DCs is unaffected by the absence of CD53, indicating that the impaired cellular immune response in *Cd53*$^{-/-}$ mice is due to an intrinsic T cell defect.

Finally, since antigen-specific T cell responses are vital to tumor elimination, we investigated cellular immunity in *Cd53*$^{-/-}$ and WT mice using the T cell-dependent tumor rejection model RMA-Muc1 (Gartlan et al., 2013; Plunkett et al., 2004). Tumor rejection by *Cd53*$^{-/-}$ mice was impaired, as the tumor burden (in mm^3) was significantly larger in *Cd53*$^{-/-}$ mice as compared with WT mice on days 14 and 17 post tumor cell inoculation (Figures 3F and 3G). These data confirm that *Cd53*$^{-/-}$ mice show impaired T cell immune responses *in vivo*.

CD53 interacts with CD45, and they colocalize at the immunological synapse

An indication of the mechanism underlying CD53 function in T cells came from our parallel investigations identifying CD53-interacting partners in lymphocytes using unbiased mass spectrometry. Analysis of CD53 complexes immunoprecipitated from Raji cell lysates revealed a protein band of large MW (200–220 kDa), which did not correspond to any known partners (Figure 4A). Although this high MW band was also visible in the

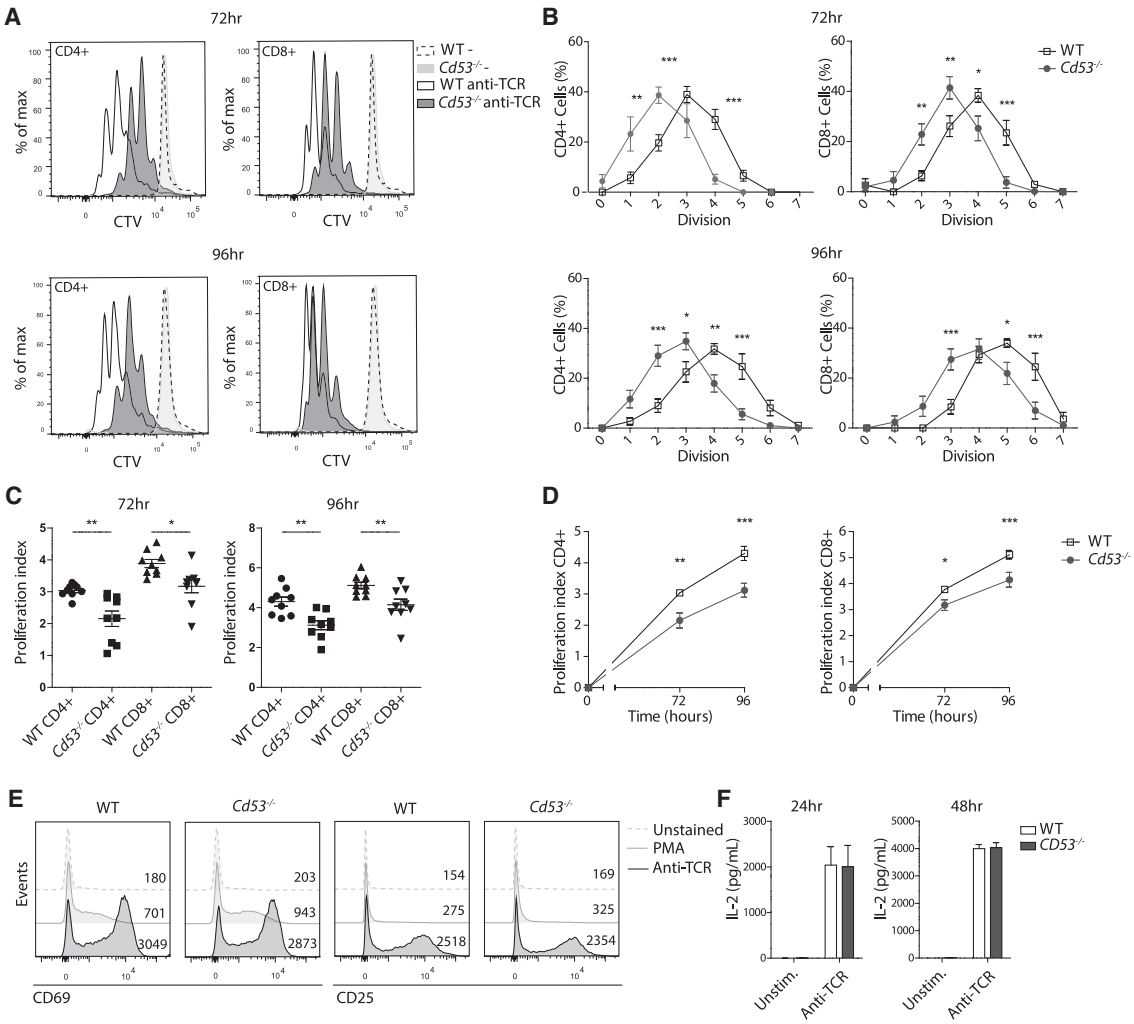

Figure 2. *Cd53*$^{-/-}$ T cells exhibit an impaired activation response

(A) CD4$^+$ and CD8$^+$ T cell proliferation measured by flow cytometry of one representative WT (dashed line) and *Cd53*$^{-/-}$ (light gray filling) mouse at 72/96 h post-stimulation with anti-CD3, and anti- CD3/CD28-stimulation (WT: solid black line, *Cd53*$^{-/-}$: dark gray filling).

(B) Percentage of CD4$^+$ and CD8$^+$ T cells per division at 72/96 h post-stimulation (WT: unfilled squares, *Cd53*$^{-/-}$: gray filled circles) (n = 9 mice/genotype from three independent experiments (mean ± SEM, two-way ANOVA)).

(C) Proliferation index of WT and *Cd53*$^{-/-}$ CD4$^+$ and CD8$^+$ T cells at 72/96 h post-stimulation (n = 9 mice/genotype from three individual experiments, mean ± SEM, unpaired two-sided t test).

(D) Data presented in (C) with changes in proliferation index shown in time for WT and *Cd53*$^{-/-}$ T cells (mean ± SEM, two-way ANOVA).

(E) Expression of CD69 and CD25 on WT and *Cd53*$^{-/-}$ T cells as measured by flow cytometry 24 h after stimulation with PMA, anti-CD3/CD28, or unstimulated (gMFI = geometric mean fluorescence intensity) (n = 6 mice/genotype from two independent experiments).

(F) IL-2 production (ELISA) for WT mice (white bars) and *Cd53*$^{-/-}$ mice (gray bars) at 24/48 h after anti-CD3/CD28 stimulation or unstimulated (n = 9–10 mice/genotype per time point from five independent experiments, mean ± SEM, unpaired two-sided t test). *p < 0.05, **p < 0.01, ***p < 0.001. See also Figure S1.

immunoprecipitation (IP) of the control tetraspanin CD81, it was clearly less strong than in the CD53 IP, indicating a preferred interaction with CD53. IPs of CD53, CD81, and CD9 were subjected to quantitative label-free mass spectrometry to identify all partners. Nonspecific hits were excluded based on their common presence in the CD9 control IP, which is not expressed by Raji cells. In addition to validating known tetraspanin partners, our analysis identified several previously unidentified protein interactions (Figure 4B; Table S1). The >200-kDa protein was identified as CD45 (PTPRC), with up to 57 peptides, including 38 unique peptides, covering 57% of the full-length isoform of CD45 detected. Importantly, there was 50 to 100 times more CD45 present in the CD53 IP compared with the CD81 IP. Of note, CD45-associating protein (CD45-AP) was also identified in one of the two CD53 IPs, but not in the CD81 IP. We confirmed these findings by performing an IP of CD53 followed by a staining for CD45, which revealed a specific band at the expected height of 200 to 220 kDa that was not observed in control IPs of CD55 and CD81 (Figure 4C). The specificity of the CD53-CD45 interaction was further verified by biotinylation of the cell

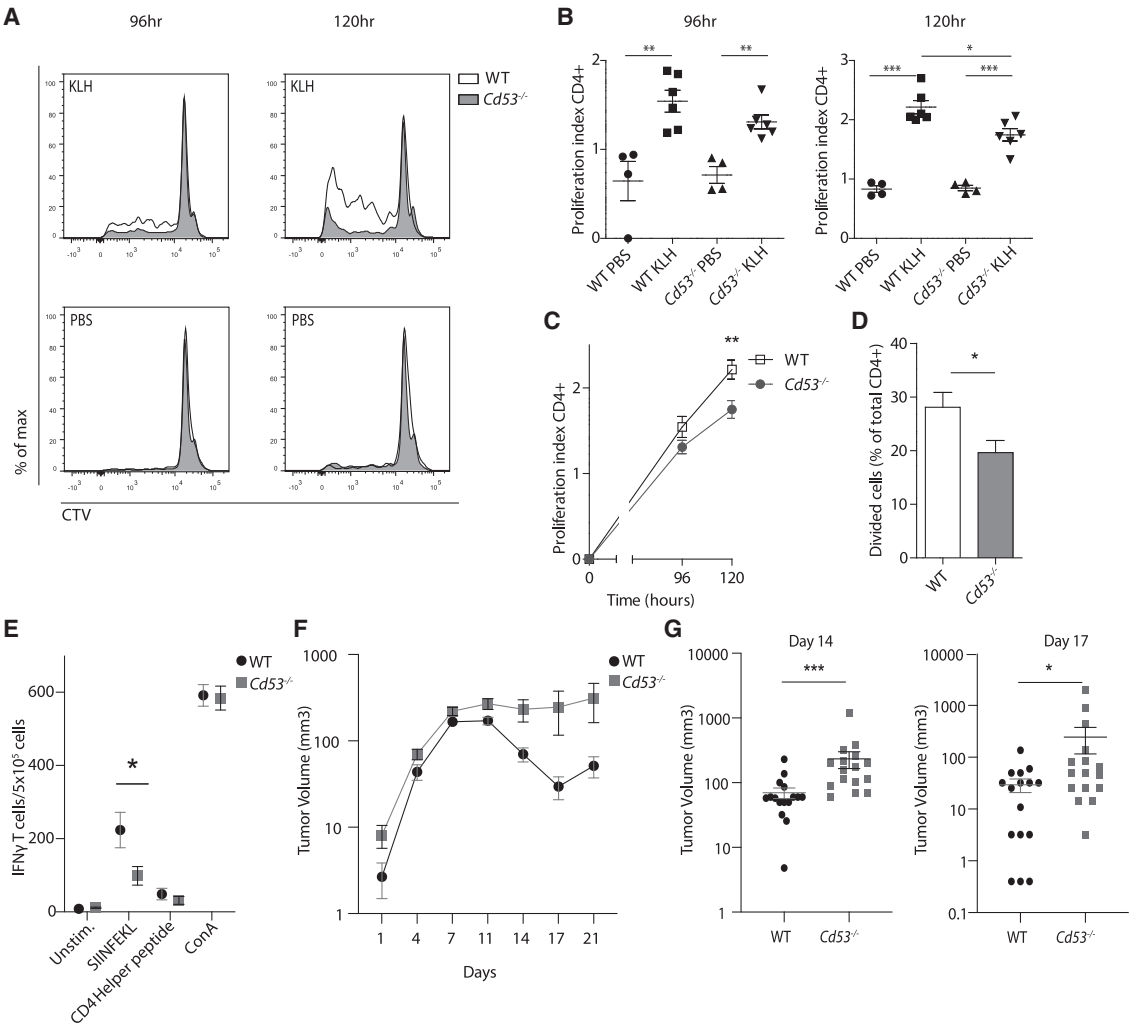

Figure 3. T cells of *Cd53*$^{-/-}$ mice are impaired in their recall response and tumor rejection capacity *in vivo*

(A) CD4$^+$ T cell proliferation measured by flow cytometry for representative WT (black line) and *Cd53*$^{-/-}$ mice (gray filled) immunized with KLH or PBS. Data from 96 and 120 h post-stimulation with KLH in the presence of naive WT antigen-presenting cells (n = 6 mice/genotype from two independent experiments).

(B) Proliferation index of CD4$^+$ T cells from PBS and KLH immunized WT and *Cd53*$^{-/-}$ mice as in (B) (n = 4–6 mice/genotype, two independent experiments, ±SEM, unpaired two-sided t test).

(C) Quantification of data presented in (B), with changes in proliferation index shown over time (mean ± SEM two-way ANOVA).

(D) Percentage of total CD4$^+$ population from KLH immunized mice entering division upon restimulation (n = 6 mice/genotype from two independent experiments (mean ± SEM, unpaired two-sided t test).

(E) Frequency of interferon-γ (IFNγ)-producing WT and *Cd53*$^{-/-}$ CD8$^+$ T cells in the total splenocyte population, measured by ELISPOT 14 days post-immunization with γ-irradiated B16OVA cells. Cells were either unstimulated or stimulated with SIINFEKL peptide, CD4 helper peptide or concanavalin A (ConA) (n = 19 mice/genotype, four independent experiments, mean ± SEM, Welch's two-sided t test).

(F) RMA-Muc1 tumor growth (in mm^3) in WT and *Cd53*$^{-/-}$ mice in time.

(G) Volume of tumors for WT and *Cd53*$^{-/-}$ mice on days 14 and 17 post tumor cell injection. (F and G) n = 16 mice/genotype, four independent experiments (mean ± SEM, Mann-Whitney *U* test). *p < 0.05, **p < 0.01, ***p < 0.001. See also Figures S1 and S2.

surface, followed by IP of CD53, CD45, and multiple control membrane proteins (tetraspanins and non-tetraspanin proteins) (Figure S3A).

Finally, we studied whether CD53 and CD45 resided within the same nanodomain by proximity ligation assays (PLA) in the human T cell line CEM. As positive control, endogenous CD45 was labeled with two different antibodies, resulting in a high number of foci per cell. Similarly, labeling of endogenous CD45 together with CD53 produced a large number of foci per cell (Figures 4D and 4E). To confirm the specificity, endogenous CD45 was labeled together with a different tetraspanin protein (CD151), as expected this combination generated fewer foci per cell (Figures 4D and 4E).

These data reveal that CD53 and CD45 reside very close to each other (<40 nm distance) on the T cell surface, indicating a direct interaction. Next, we investigated whether this interaction

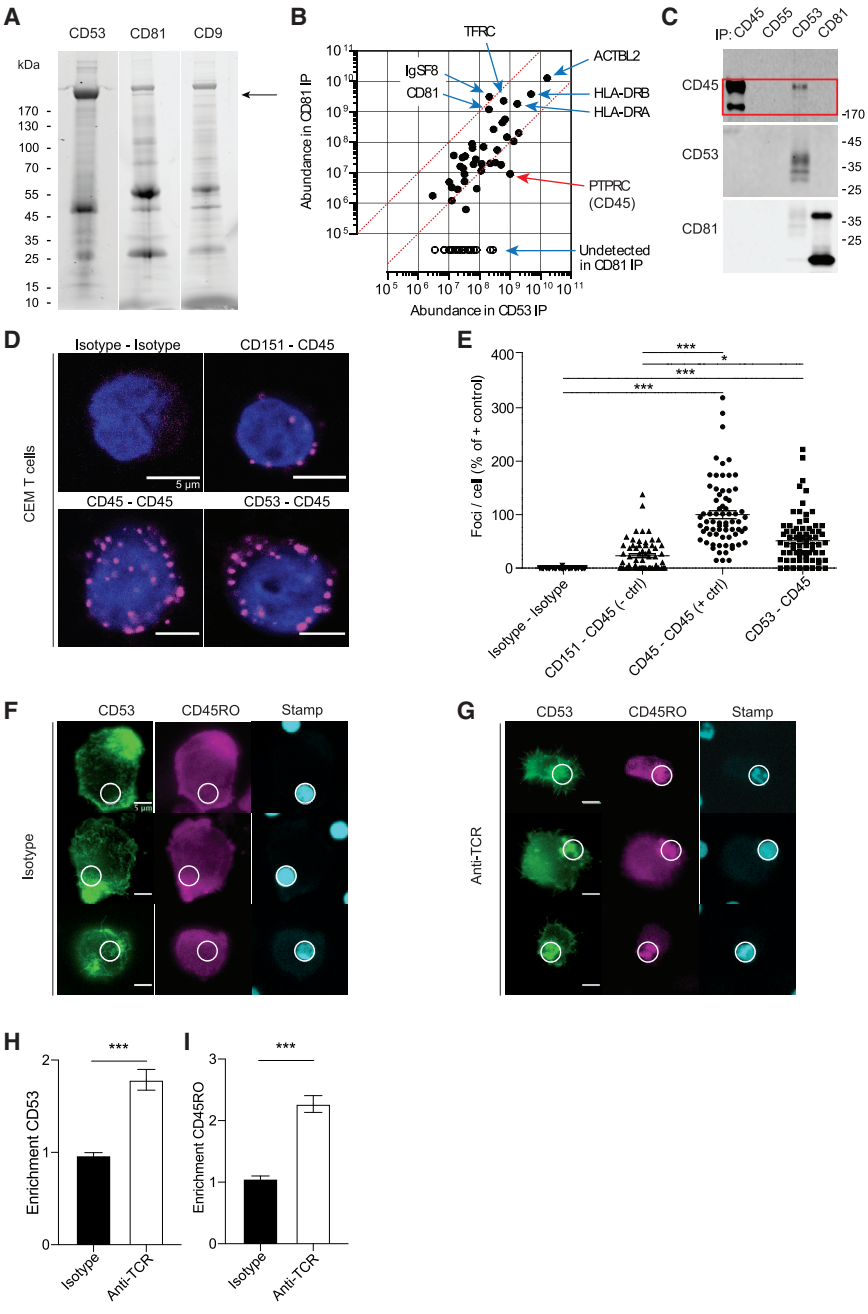

Figure 4. CD53 interacts with CD45, and they colocalize at the immunological synapse

(A) Coomassie-stained SDS-PAGE gel showing IPs of CD53, CD81, and CD9 in Raji B cells. Arrow indicates interacting protein of 200 to 220 Kd corresponding with CD45.

(B) Scatterplot shows relative protein abundance of co-immunoprecipitated proteins identified by label-free mass spectrometry for CD53 IP compared with CD81 IP. IP of CD9 was used to identify and exclude aspecific proteins. Arrows indicate specific proteins of interest in the scatterplot as well as proteins exclusively interacting with CD53. Complete list in Table S1. CD53 IP values are based on means from two independent experiments.

(C) Western blot of CD45, CD55, CD53, and CD81 IPs stained with an anti-CD45 antibody. Red box indicates the expected location of the CD45 band.

(D) Microscopy images of PLA on human CEM T cells, showing Isotype-Isotype, CD151-CD45 (negative control), CD45-CD45 (positive control), or CD53-CD45 labeling. PLA-foci in magenta, nuclear labeling in blue. Scale bars, 5 µm.

(E) Quantification of PLA conditions in human CEM T cells as shown in (D). Percentage of foci/cell was determined by normalizing to CD45-CD45 (n > 60 cells/condition, two independent experiments, mean ± SEM, Kruskal-Wallis test).

(F) Images of CEM T cells transfected with sGFP2-CD53 and CD45RO-mCherry on anti-CD3/CD28 antibody prints. Specific enrichment of CD53 and CD45RO is shown at the antibody prints, indicated with a white circle, but not on isotype control prints (G). Scale bars, 5 µm.

(H and I) Quantification of CD53 or CD45RO enrichment in CEM T cells from data of (E) and (F). Fold-change was determined by normalizing enrichment at the antibody print-site to enrichment at an unprinted-site of equal size (n = 40 cells/condition, three independent experiments, mean ± SEM, unpaired two-sided t test). *p < 0.05, **p < 0.01, ***p < 0.001. See also Figures S3 and S4.

was also maintained at the immune synapse, where the main function of CD45 is executed. We hypothesized that if CD53 was important for CD45 function during T cell activation, these proteins would both be simultaneously recruited to the immune synapse. Microcontact printing was used to create localized areas for TCR engagement using CD3/CD28 antibodies (anti-TCR), or isotype antibodies as a control (van den Dries et al., 2012; Zuidscherwoude et al., 2017). Both CD45RO and CD53 were recruited simultaneously and specifically to the site of TCR engagement in contrast to isotype controls (Figures 4F and 4G). Quantification confirmed significant enrichment of both CD45RO and CD53 at the anti-TCR print compared with the isotype control (Figures 4H and 4I). To evaluate the specificity, control experiments were performed with CD37, another immune-specific tetraspanin. Clear enrichment of CD53, but not of CD37, was observed upon TCR engagement in these T cells (Figures S4A–S4D). Finally, based on our previous study that demonstrated an interaction between CD53 and protein kinase C (PKC) β in B cells, we investigated whether such an interaction was also present in T cells (Zuidscherwoude et al., 2017) by studying PKCθ, the main isoform in T cells, using microcontact printing and fluorescence lifetime imaging microscopy (FLIM). We observed significant enrichment of PKCθ at anti-TCR prints, but not at the isotype control prints (Figures S4E and S4F). However, no decrease in donor lifetime was observed upon PKCθ

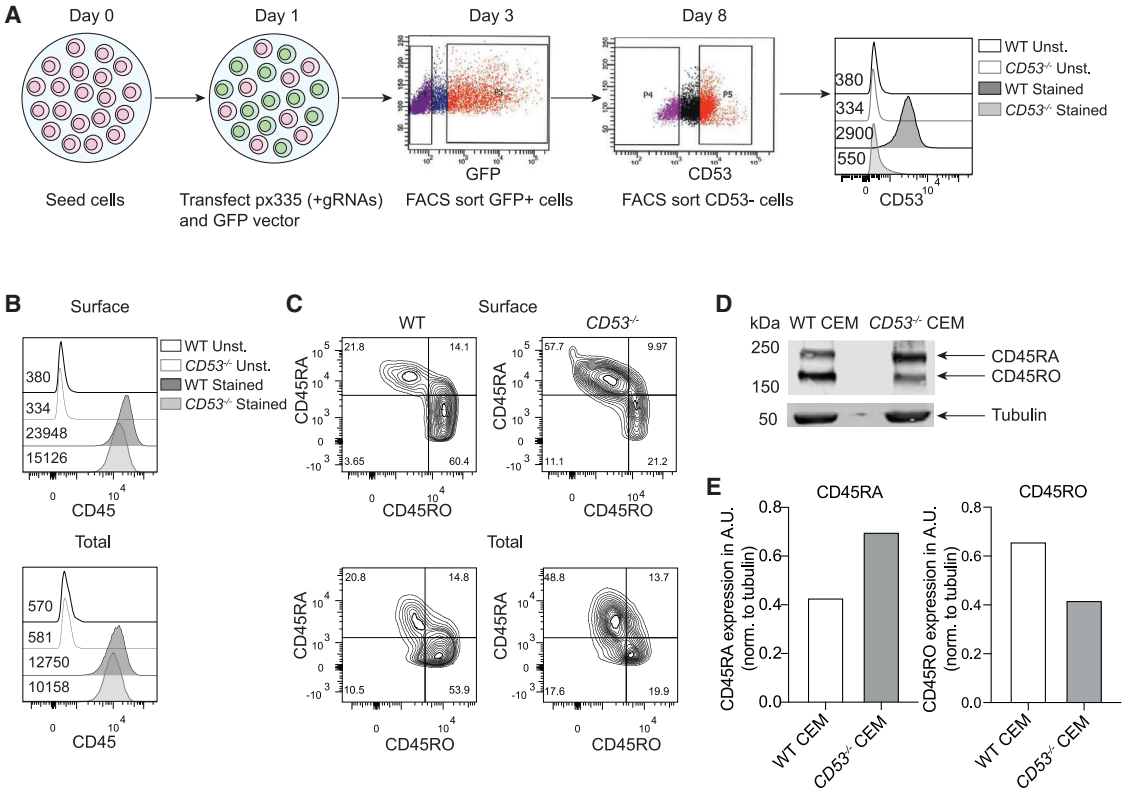

Figure 5. CD45 isoform expression pattern is distorted by loss of CD53

(A) Overview of generation of human polyclonal CD53 knockout CEM T cell line through CRISPR-Cas9-mediated gene editing. CD53 expression measured by flow cytometry (values in gMFI).

(B) Surface and total expression of CD45 in WT and *CD53*$^{-/-}$ T cells measured by flow cytometry (values in gMFI from one representative experiment, three independent experiments were performed yielding similar results).

(C) Two-parameter zebra plots showing surface and total expression of CD45RA and CD45RO in WT and *CD53*$^{-/-}$ T cells from one representative experiment. Three independent experiments were performed yielding similar results.

(D) Immunoblot of WT and *CD53*$^{-/-}$ T cells probed for CD45RO and CD45RA. Tubulin is shown as loading control. Arrows indicate relevant bands.

(E) Quantification of bands shown in (D), CD45RA and CD45RO signals were normalized to tubulin. See also Figure S5.

translocation to the membrane, indicating that while PKCθ is recruited to the TCR upon signaling, it does not interact directly with CD53 (Figure S4G). Thus, unlike in B cells, in T cells CD53 was not found to interact with PKC, excluding this as an explanation for the impaired T cell activation in the absence of CD53.

Taken together, these data show a direct interaction between CD53 and the protein tyrosine phosphatase CD45 in T cells. CD45 and CD53 were found to localize contemporaneously at the immunological synapse during TCR stimulation, suggesting a possible role for CD53 in the regulation of CD45 function.

CD45 isoform expression pattern is distorted by loss of CD53

To understanding the functional interaction between CD53 and CD45, we engineered a human *CD53*$^{-/-}$ T cell line (CEM) using CRISPR/Cas9 technology (Figure 5A). A general characterization of the *CD53*$^{-/-}$ T cell line revealed normal surface expression of CD3, CD4 and CD28 comparable to the CD53-positive parental T cell line (WT) (Figure S5A).

Next, we assessed the expression of CD45, CD45RO, and CD45RA in *CD53*$^{-/-}$ and WT T cells. Remarkably, an overall decrease in the expression of CD45 was observed upon loss of CD53. More striking was the difference observed in the expression patterns of CD45RA and CD45RO between *CD53*$^{-/-}$ and WT T cells (Figures 5B and 5C). WT T cells were found to be largely CD45RO-positive (~60%), with a smaller population (~20%) of CD45RA-positive cells. This profile was inverted in *CD53*$^{-/-}$ T cells, which showed a small population of CD45RO-positive T cells (~20%), and a larger CD45RA-positive population (~50%–60%), which was confirmed by quantitative western blot analysis of CD45 isoform expression (Figures 5D and 5E). Overall, these results indicate a significant change in CD45 isoform expression induced by the loss of CD53. This led us to hypothesize that CD53 may be required for the stabilization of CD45RO at the plasma membrane.

CD53 regulates the mobility and stability of CD45RO on the T cell surface

To investigate whether CD53 was required for stable CD45RO expression, we performed CD45 internalization assays on *CD53*$^{-/-}$ and WT T cells. Because *CD53*$^{-/-}$ and WT T cells express disparate levels of CD45RO and CD45RA, both WT and

CD53$^{-/-}$ CEM T cells were transiently transfected with either CD45RO-mCherry or CD45RA-mCherry to achieve comparable CD45 surface expression levels. Internalization of CD45RO was observed to be significantly higher in *CD53*$^{-/-}$ T cells as compared with WT T cells, with 53% of *CD53*$^{-/-}$ T cells still expressing CD45RO at 24 h compared with 75% of WT T cells (Figures 6A and 6B). Interestingly, in contrast to CD45RO, no differences in internalization were observed for CD45RA between *CD53*$^{-/-}$ and WT T cells (Figures 6C and 6D). These data indicate that CD53 is involved in membrane stabilization of CD45RO, but not of CD45RA.

To investigate the consequences of CD45RO instability, we used fluorescence recovery after photo bleaching (FRAP) to study CD45RO mobility. *CD53*$^{-/-}$ and WT T cells were both transiently transfected with CD45RO-sGFP2 to ensure similar expression levels. Cells were then subjected to FRAP analysis and recovery curves were acquired (Figures 6E and 6F). Quantification revealed that in the absence of CD53, CD45RO was significantly more mobile on the T cell surface (Figure 6G). To investigate whether this was specific to CD45RO, the mobility of CD45RA was analyzed (Figures 6H and 6I). In contrast to CD45RO, no significant difference in the mobile fraction of CD45RA was seen between WT and *CD53*$^{-/-}$ T cells, indicating isoform-specific regulation by CD53 (Figure 6J). Taken together, our results show that in the absence of CD53, CD45RO becomes unstable on the T cell surface, as evidenced by its increased internalization and mobility, which is not seen for CD45RA.

Loss of CD53 impairs the function of CD45

Since mobility can affect localization and function, we postulated that in the absence of CD53, CD45 function may be impaired. TCR signaling activity was first investigated in *CD53*$^{-/-}$ and WT CEM T cells upon stimulation with anti-TCR antibodies. Total phosphorylated tyrosine (pTyr) signal increased in both WT and *CD53*$^{-/-}$ CEM T cells upon stimulation, confirming successful TCR stimulation (Figure 7A). Quantification of a higher MW (120 kDa) and a lower MW (37 kDa) band revealed significantly higher tyrosine phosphorylation in WT cells compared with *CD53*$^{-/-}$ T cells at 2 min post-stimulation (Figures 7B and 7C). In addition, phosphorylation of the CD3 zeta chains (pCD3z) at position tyrosine 142 (Y142), a specific target of Lck, was significantly higher in WT T cells compared with the *CD53*$^{-/-}$ T cells (Figure 7D). Next, TCR signaling activity was studied in primary murine WT and *Cd53*$^{-/-}$ T cells. Although total pTyr signal was not different between murine WT and *Cd53*$^{-/-}$ T cells upon TCR stimulation (Figure S6), phosphorylated targets of CD45 were differentially activated in WT and *Cd53*$^{-/-}$ T cells. We first analyzed phosphorylation of Lck at positions tyrosine 394 (Y394) and 505 (Y505), since Lck is directly targeted by CD45 in T cells, using phospho-flow cytometry (Figures 7E and 7G). Lck Y394 and Y505 phosphorylation were measured under basal conditions, as multiple studies have shown that TCR stimulation does not lead to a significant increase in Lck activation per se, and that basal phosphorylation is therefore a more robust readout for Lck activity (McNeill et al., 2007; Nika et al., 2010; Wei et al., 2020). We observed that *Cd53*$^{-/-}$ T cells have significantly lower phosphorylation of Y394, which confirms that the absence of CD53 in T cells leads to compromised CD45 function, as Y394 is the dominant phosphorylation site for Lck (Nika et al., 2010; Wei et al., 2020) (Figure 7F). Phosphorylation of Y505 was not significantly different between WT and *Cd53*$^{-/-}$ T cells (Figure 7H). To assess the impact of dysfunctional Lck activation in *Cd53*$^{-/-}$ T cells on TCR signaling directly, we measured the pCD3z (Y142) (Figure 7I). Our results show that *Cd53*$^{-/-}$ T cells have significantly less phosphorylation at Y142 compared with WT cells upon CD3/CD28 stimulation (Figure 7J). This was the case for both the CD4^{+} and CD8^{+} T cell compartments. In addition, to confirm altered CD45 activity in *Cd53*$^{-/-}$ T cells through an independent assay, we used the pCap-SP1 peptide probe to specifically measure CD45 activity by flow cytometry (Stanford et al., 2012; Szodoray et al., 2016). pCap-SP1 probe fluorescence measurements revealed a clear difference in CD45 activity between *Cd53*$^{-/-}$ and WT T cells upon TCR stimulation (Figure 7K). Quantification of these results over multiple experiments revealed a significantly reduced CD45 activity in *Cd53*$^{-/-}$ T cells as compared with WT T cells (Figure 7L). Finally, we analyzed the dimerization capacity of CD45, which has been proposed to regulate CD45 function (Xu and Weiss, 2002). Western blots were performed on WT and *CD53*$^{-/-}$ T cell samples either untreated or treated with sulfo-EGS to crosslink CD45 dimers and stained for CD45 (Figure S7A). Calculating the amount of CD45 contained in dimers as a percentage of total CD45 revealed no differences between WT and *CD53*$^{-/-}$ T cells (Figure S7B).

Taken together, our results show that the overall function of CD45 is impaired, as activated *Cd53*$^{-/-}$ T cells show a clear defect in overall tyrosine phosphorylation, CD3 zeta chain and Lck phosphorylation, and CD45 activity compared with WT T cells.

DISCUSSION

Since its discovery in the 1970s, CD45 has been of great interest because of its leukocyte-specific distribution pattern and high abundance on the T cell surface (Fabre and Williams, 1977; Trowbridge, 1978; Zikherman et al., 2010). The importance of CD45 in TCR signaling and T cell activation, as exemplified by the more pronounced T cell phenotype versus B cell phenotype in CD45-deficient mice, is now well recognized, yet many questions remain regarding the regulation of CD45 at the T cell surface. The KS model proposes that physical exclusion of CD45 from TCR nanoclusters is needed to support sustained signaling leading to T cell activation (Cordoba et al., 2013). Paradoxically, close proximity between CD45 and the TCR is a requirement for the activation of Lck and initiation of TCR signaling (Courtney et al., 2019; Furlan et al., 2014). Thus, T cell activation depends both on TCR interaction with, and separation from, CD45. Moreover, the specific relative positioning of CD45 and the TCR has been proposed to regulate signaling, indicating that tight control over membrane organization is required for optimal T cell activation (Razvag et al., 2018). Recently, selective pre-exclusion of CD45 from T cell microvilli prior to APC engagement has been observed, which challenges the classic KS model and highlights the complexity involved in the regulation of CD45 localization (Jung et al., 2021). Thus, since CD45 activity is mainly determined by its localization, mechanisms controlling the lateral

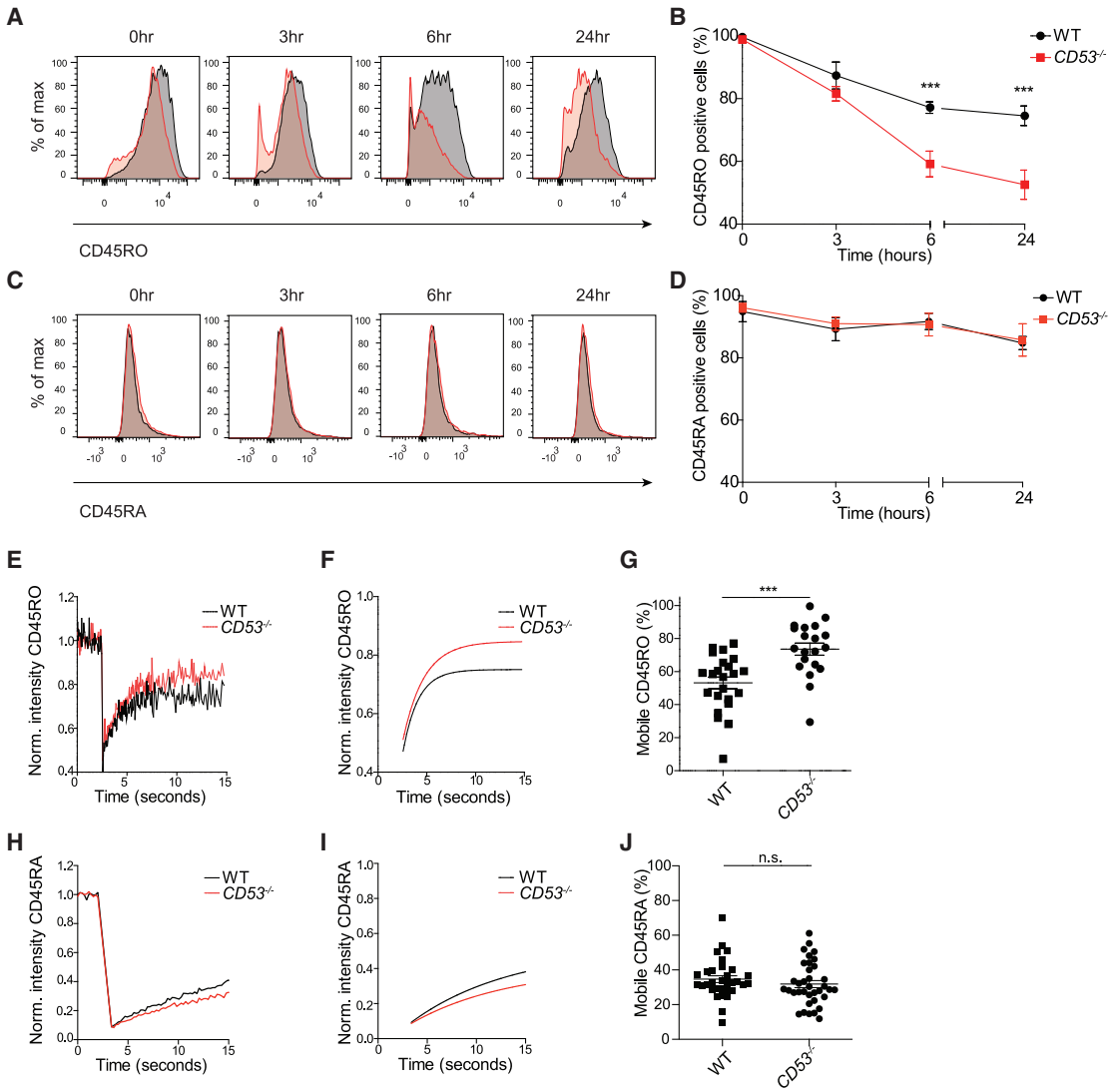

Figure 6. CD53 regulates the mobility and stability of CD45RO on the T cell surface

(A) Internalization of CD45RO over time measured by flow cytometry. Filled black and red graphs denote WT and *CD53*$^{-/-}$ CEM T cells, respectively, gated on mCherry expression.

(B) Quantification of the internalization of CD45RA expressed as % of CD45RA-positive cells over time (n = 3 independent experiments, mean ± SEM, two-way ANOVA).

(C) Internalization of CD45RA over time as measured by flow cytometry as in (A).

(D) Quantification of the internalization of CD45RA expressed as % of CD45RA-positive cells over time (n = 3 independent experiments, mean ± SEM, two-way ANOVA).

(E) FRAP recovery curves obtained for CD45RO in WT and *CD53*$^{-/-}$ CEM T cells. Curve represents the average of all cells (>10) from one representative experiment.

(F) Biexponential decay fit of the curve obtained in (E) as calculated by OriginPro8 software program.

(G) Percentage of mobile CD45RO as calculated based on FRAP curves (n > 20 cells/genotype from three independent experiments, mean ± SEM, unpaired two-sided t test).

(H) FRAP recovery curves obtained for CD45RA in WT and *CD53*$^{-/-}$ CEM T cells. Curve represents the average of all cells (>10) from one representative experiment.

(I) Biexponential decay fit of the curve obtained in (E) as calculated by OriginPro8 software program.

(J) Percentage of mobile CD45RA as calculated based on FRAP curves (n > 20 cells/genotype from three independent experiments, mean ± SEM, unpaired two-sided t test). ***$p < 0.001$.

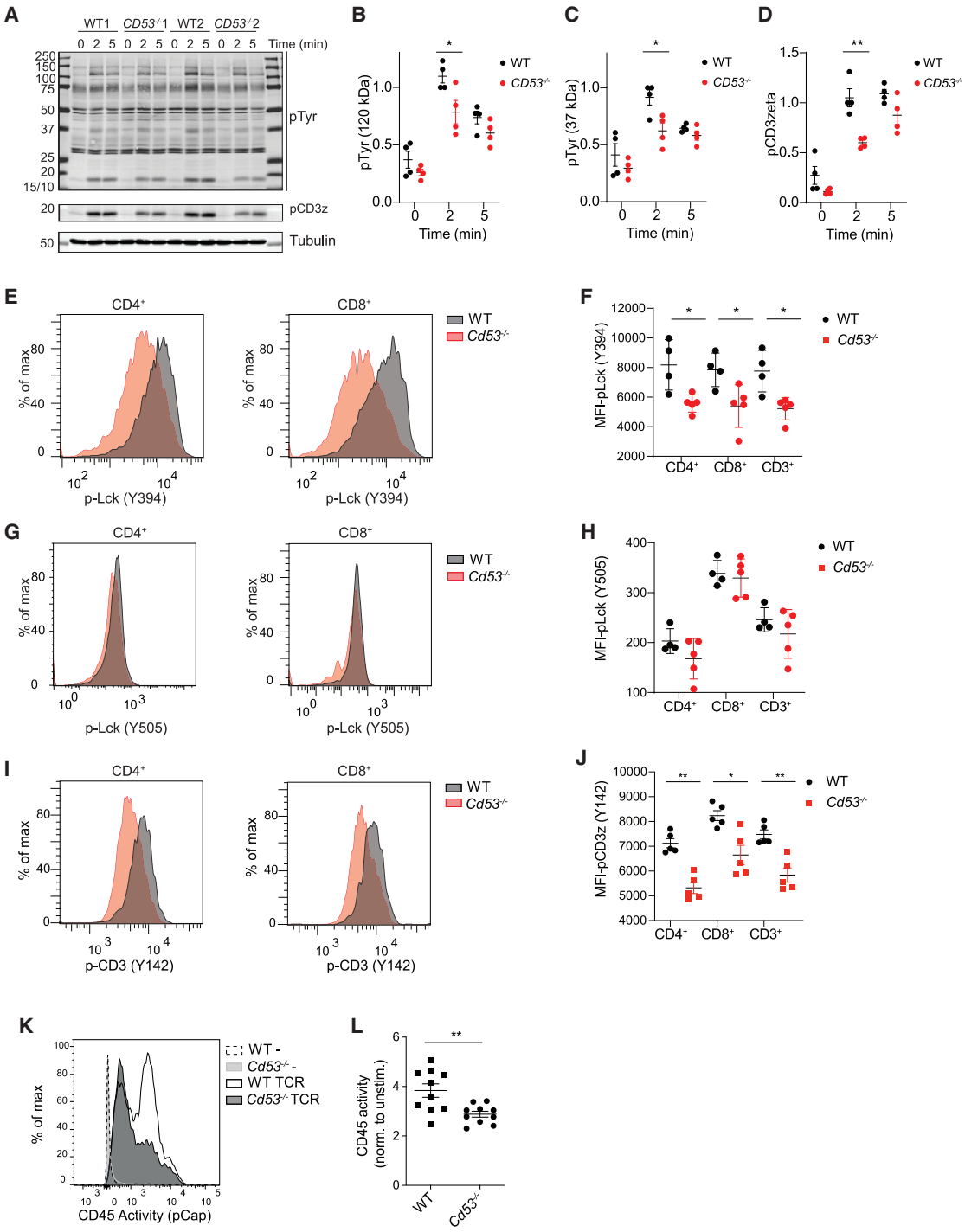

Figure 7. Loss of CD53 impairs the function of CD45

(A) Immunoblot of WT and *CD53*$^{-/-}$ CEM T cells unstimulated or stimulated with anti-TCR antibodies for 2 or 5 min. Blot was probed for total phosphorylated tyrosine (pTyr), phosphorylated CD3 zeta chains (pCD3z), and tubulin loading control. One representative immunoblot showing two replicates for each genotype is shown. Quantification is based on n = 4 per genotype, two independent experiments.

(B) Graph shows the quantification of a pTyr band at 120 kDa as shown in (A), normalized to tubulin intensity (n = 4, two independent experiments, mean ± SEM, t test).

(C) Graph shows the quantification of a pTyr band at 37 kDa as shown in (A), normalized to tubulin intensity (n = 4, two independent experiments, mean ± SEM, t test).

(D) Graph shows the quantification of the pCD3z band as shown in (A), normalized to tubulin intensity (n = 4, two independent experiments, mean ± SEM, t test).

(legend continued on next page)

mobility and dynamic spatiotemporal regulation of CD45 must play an important role in T cell activation. Adding to the complexity, the specific regulation of CD45 isoforms on the T cell surface, which remains to be elucidated, must also be acknowledged.

Here, we identify the tetraspanin CD53 as key regulator of CD45 in T cells using a combination of *in vivo* assays, unbiased mass spectrometry, imaging techniques, and biochemical assays. Investigation into the mechanism revealed that CD53 regulates CD45 function on the T cell surface, is essential for the stability of CD45RO, and controls CD45RO mobility. Tetraspanins function not as classical receptors, but by interacting with other membrane proteins *in cis*. Membrane protein organization induced by tetraspanins is emerging as an important mechanism to control immune receptor function (Cabañas et al., 2019; Van Deventer et al., 2017). Other mechanisms that have been proposed to regulate CD45 localization on the T cell membrane include partitioning into lipid rafts and interactions with the cytoskeleton or with galectins (Cairo et al., 2010; Chen et al., 2007; Pradhan and Morrow, 2002; Zhang et al., 2005).

We find that the removal of CD53 results in the loss of CD45RO expression, altering the expression pattern of CD45 isoforms and diminishing T cell activation. CD45 isoform switching occurs during normal T cell activation, yet the purpose of this process remains largely unclear. The importance of isoform-specific CD45 regulation is exemplified by studies showing that the combinations of expressed CD45 isoforms determine T cell responses (Dawes et al., 2006). Others have shown isoform-dependent differences in downstream signaling, although sometimes with contradictory outcomes (Chui et al., 1994; Dornan et al., 2002; Krummey et al., 2020; Novak et al., 1994; Shanafelt et al., 1996). Recently, it has been shown that isoforms of CD45 can segregate differently during TCR-MHC interaction, suggesting this as a mechanism for the fine-tuning of signaling (Carbone et al., 2017). Thus, multiple studies support isoform-specific functions for CD45 in T cells, and our findings now demonstrate CD45 isoform-specific expressional regulation, stabilization, and mobility through interaction with the tetraspanin CD53. Although we show that CD53 affects stabilization and mobility of CD45RO specifically, the involvement of other CD45 isoforms cannot be excluded. Based on its relatively small size, CD53 most likely interacts with a membrane-proximal domain common to all CD45 splice variants. Our finding that CD53 is important for the stabilization and mobility of CD45RO, but not CD45RA, may indicate the involvement of other isoform-specific partners. Alternatively, glycosylation is important for CD45 stability and transport to the cell membrane (Pulido and Sánchez-Madrid, 1992). As the shortest variant of CD45, CD45RO is the least glycosylated isoform, this may result in the need for additional stabilization at the cell surface that could be provided by CD53. Based on our results, we can exclude an effect of CD53 on CD45 dimerization, which has been proposed to be more rapid and efficient in CD45RO compared with other isoforms (Xu and Weiss, 2002).

The functional consequences of CD53-CD45 interaction for T cell biology are multiple. First, in the absence of CD53, primary murine T cells exhibit impaired proliferation, and primary human T cells are readily activated by the combined CD3-CD53 stimulation, resulting in proliferation and naive to effector transition. This was independent of CD28 co-stimulation, which is known to stabilize IL-2 mRNA and increase IL-2 production 30- to 100-fold (Gonsky et al., 1999; Umlauf et al., 1995). This positive role for CD53 in T cell activation is in stark contrast to other tetraspanins (CD37, Tssc6, CD81 and CD151), which all inhibit T cell proliferation through incompletely resolved mechanisms (Seu et al., 2017; van Spriel et al., 2004; Tarrant et al., 2002).

Second, *Cd53*$^{-/-}$ T cells have a reduced capacity to mount recall responses after immunization, defective IFN-γ production, proliferation, and impaired anti-tumor responses in *Cd53*$^{-/-}$ mice. Our data fit with previous findings of SCID and cancer development in patients with dysfunctional CD45, and in patients with a CD53 deficiency, who suffer from recurrent infections (Kung et al., 2000; Majeti et al., 2000; Mollinedo et al., 1997; Porcu et al., 2012; Roberts et al., 2012; Tchilian et al., 2001).

Third, we observed that CD53 deficiency influences the phosphatase function of CD45. CD53-deficient T cells showed a reduced tyrosine phosphorylation upon TCR stimulation, and impaired CD45 activity compared with WT T cells. Importantly, Lck, the main target of CD45, had reduced activity in *Cd53*$^{-/-}$ T cells as indicated by phosphorylation at Y394 and Lck probe activity compared with WT T cells. We observed that the inhibitory site Y505 was not significantly altered by CD53; however, Y505 phosphorylation status is known to be less indicative of Lck activity than Y394 phosphorylation (Nika et al., 2010; Wei et al., 2020). Moreover, while Y505 is known to be dephosphorylated by CD45 upon TCR stimulation, others have shown that during early TCR signaling, both Y394 and Y505 show increased phosphorylation (Nyakeriga et al., 2012). This indicates that the phosphorylation status of Y505 is subject to complex regulation beyond just CD45, making it difficult to assess, especially during

(E) Flow cytometry graphs showing the expression of phosphorylated Lck at position Y394 in CD4$^+$ (left) and CD8$^+$ (right) WT (black lines) and *Cd53*$^{-/-}$ T cells (red lines).
(F) Quantification of Y394 phosphorylation in WT and *Cd53*$^{-/-}$ CD4$^+$, CD8$^+$, and total T cells (n = 4–5 mice per genotype, mean ± SEM, Mann-Whitney *U* test).
(G) Flow cytometry graphs showing the expression of phosphorylated Lck at position Y505 in CD4$^+$ (left) and CD8$^+$ (right) WT (black lines) and *Cd53*$^{-/-}$ T cells (red lines).
(H) Quantification of Y505 phosphorylation in WT and *Cd53*$^{-/-}$ CD4$^+$, CD8$^+$, and total T cells (n = 4–5 mice per genotype, mean ± SEM, Mann-Whitney *U* test).
(I) Flow cytometry graphs showing the expression of phosphorylated CD3 zeta chains at position Y142 in CD4$^+$ (left) and CD8$^+$ (right) WT (black lines) and *Cd53*$^{-/-}$ T cells (red lines), isotype shown in gray.
(J) Quantification of Y142 phosphorylation in WT and *Cd53*$^{-/-}$ CD4$^+$, CD8$^+$, and total T cells (n = 5 mice per genotype, mean ± SEM, Mann-Whitney *U* test).
(K) CD45 activity in WT and *Cd53*$^{-/-}$ T cells as measured by flow cytometry assessed by CD45 probe (pCap-SP1 peptide) fluorescence. Experiments were repeated three times yielding similar results (n = 3).
(L) Quantification of CD45 activity in WT and *Cd53*$^{-/-}$ T cells as measured by flow cytometry (n = 10 mice/genotype from three independent experiments, mean ± SEM, unpaired two-sided t test). *$p < 0.05$, **$p < 0.01$.

early TCR signaling. In line with this, a known patient mutation of CD45 leading to altered isoform expression (similar to our *CD53*$^{-/-}$ phenotype) resulted in only a marginal difference in Y505 phosphorylation (<20%), despite producing a distinct phenotype in T cells (Pokoyski et al., 2015). Finally, it is well known that Lck Y505 phosphorylation status is the result of a balance between dephosphorylation by CD45 and phosphorylation by the Csk tyrosine kinase (Palacios and Weiss, 2004; Zikherman et al., 2010). Interestingly, we observed Csk kinase to be specifically enriched in our CD53-IPs, together with Lck and CD45, possibly indicating a complex interplay between these proteins that may dynamically alter Y505 phosphorylation during T cell signaling (Table S1). Importantly, our data confirmed the overall change in Lck activity through Y394 to be functionally relevant, as a direct target of Lck, the CD3 zeta chains of the TCR, also exhibited reduced activatory phosphorylation in *Cd53*$^{-/-}$ T cells. This indicates that the absence of CD53 alters Lck activity, and loss of CD53 impairs the ability of T cells to signal. Our findings are supported by an older study that showed that CD53 interacts with an unknown tyrosine phosphatase capable of dephosphorylating Lck, although this phosphatase was not identified as CD45 (Carmo and Wright, 1995). We posit that when CD53 is absent, CD45RO becomes unstable on the surface of T cells, which leads to an impaired overall CD45 function and decreased T cell activation and proliferation.

These findings not only shed light on the specific regulation of CD45, but also help clarify the role of membrane organization in T cell function. Membrane organization has been shown to aid in the coordination of the highly complex signaling processes occurring upon TCR activation (He and Bongrand, 2012). This is particularly important during the formation of the immunological synapse, when TCR nanoclusters coalesce into microclusters. Previously, we reported that CD53 controls the localization of PKC to the plasma membrane in B cells upon BCR activation (Zuidscherwoude et al., 2017), which was not the case for T cells. Thus, while in B cells CD53 regulates kinase function, in T cells CD53 regulates phosphatase activity. These opposed functions, in such closely related cell types, serve to highlight the versatility of CD53. More importantly, our findings reinforce the concept that the regulation of localization and spatial dynamics by membrane organizing proteins is a vital aspect of lymphocyte signaling.

In conclusion, we report that CD53 is a partner of the tyrosine phosphatase CD45 on the surface of T cells. CD53 is required for optimal CD45 phosphatase activity, T cell activation, and proliferation. Importantly, CD53-negative T cells are defective, both *ex vivo* and *in vivo*, including impaired T cell-mediated anti-tumor immunity. Overall, our findings provide better insight into the molecular mechanisms by which CD45 is regulated, and positions CD53 as key regulator of CD45RO in T cells. These findings may facilitate development of better methods to modulate T cell activity and treat T cell-dependent diseases such as autoimmunity and cancer.

Limitations of the study

Although our experiments establish a role for CD53 in T cell immunity through the regulation of CD45 stability, mobility, and function, our studies do not reveal (1) which specific CD45 isoform(s) interact with CD53, (2) whether CD53 and CD45 interact in isolation or as part of a larger complex, and (3) which domains of each protein are responsible for the interaction.

STAR★METHODS

Detailed methods are provided in the online version of this paper and include the following:

- KEY RESOURCES TABLE
- RESOURCE AVAILABILITY
  - Lead contact
  - Materials availability
  - Data and code availability
- EXPERIMENTAL MODEL AND SUBJECT DETAILS
  - Animals
  - Cells
- METHOD DETAILS
  - Isolation of human primary T cells
  - Isolation of murine primary T cells
  - T cell proliferation assays (human and murine)
  - IL-2 ELISA
  - KLH immunizations and ex-vivo recall assay
  - Differentiation of BMDCs from WT and *Cd53*$^{-/-}$ mice
  - Assessing MHC-I and MHC-II expression on primary murine spleen-derived dendritic cells
  - *In vitro* antigen presentation assay
  - *In vivo* antigen presentation assay
  - RMA-Muc1 tumor rejection model
  - B16-OVA tumor cell immunization and ELISPOT
  - Cell labeling, immunoprecipitation, and mass spectrometry
  - Immunoprecipitation and CD45 staining
  - Proximity Ligation Assays
  - Micro-contact printing
  - Transfection and fluorescence lifetime imaging microscopy (FLIM)
  - Generation of human polyclonal CD53-deficient CEM T cells by CRISPR/Cas9-mediated genome editing
  - FRAP of WT and *CD53*$^{-/-}$ CEM T cells
  - CD45 internalization assay
  - Western blot CD45 isoform expression
  - Western blot CD45 dimerization
  - Western blot for p-Tyr and pCD3 zeta (Y142)
  - Phospho-flow of CD3 zeta chains and Lck
  - CD45 activity assay
- QUANTIFICATION AND STATISTICAL ANALYSIS

SUPPLEMENTAL INFORMATION

Supplemental information can be found online at https://doi.org/10.1016/j.celrep.2022.111006.

ACKNOWLEDGMENTS

We thank the Central Animal Laboratory of Nijmegen (CDL) and the Microscope Imaging Center of the Radboudumc for their support and assistance. We acknowledge funding support from the Netherlands Organization for Scientific Research (NWO): the Institute of Chemical Immunology (project

024.002.009 and ICI 000-23 to S.J.v.D. and A.B.v.S.), VIDI (project 864.11.006) to A.B.v.S., ZonMW (project 09120012010023) to A.B.v.S., the Dutch Cancer Society (KUN2014-6845, 11618 to L.Q.C. and A.B.v.S., 12949 to A.B.v.S.), and the European Research Council: Consolidator Grant (project 724281) to A.B.v.S.

AUTHOR CONTRIBUTIONS

V.M.E.D. designed, performed, and analyzed most experiments including human and murine T cell characterization and proliferation assays, KLH immunization assays, microcontact printing, FLIM, FRAP, western blotting, and CD45 activity assays. A.B.A., E.J., and A.B.v.S. assisted in processing and isolation of primary murine T cells. A.B.A. performed and analyzed flow cytometry of thymic T cells, proximity ligation experiments, and FRAP. S.P.S. set up and analyzed phospho-flow experiments. E.J. measured human and murine T cell cytokine production by ELISA. S.C., V.N.G., and E.R. immunoprecipitated tetraspanins with CD45 and performed the mass spectrometry. A.B.A. and S.J.v.D. generated the *CD53*$^{-/-}$ CEM T cell line. F.S. assessed the RMA-Muc1 tumor growth in WT and *Cd53*$^{-/-}$ mice and preformed the *in vitro* and *in vivo* antigen presentation assays. M.T.B. performed the western blots for CD45 dimerization and pTyr phosphorylation experiments. M.Z. measured the expression MHC-I and MHC-II on primary splenic dendritic cells (DCs) and generated bone marrow-derived DCs from WT and *Cd53*$^{-/-}$ mice to characterize the DC subset distribution. B.N. and P.S. provided the pCap-SP1 peptide and protocol for the assessment of CD45 activity. M.C.D. and M.D.W. performed the immunization of WT and *Cd53*$^{-/-}$ mice with γ-irradiated B16OVA cells and measured T cell responses by ELISPOT. A.B.v.S. together with L.C.Q. supervised the project and provided resources and expertise. V.M.E.D. designed the figures and wrote the manuscript with help from A.B.A., L.C.Q., and A.B.v.S.

DECLARATION OF INTERESTS

The authors declare no competing interests.

Received: July 1, 2021
Revised: May 2, 2022
Accepted: June 3, 2022
Published: June 28, 2022

REFERENCES

Birkeland, M.L., Johnson, P., Trowbridge, I.S., and Puré, E. (1989). Changes in CD45 isoform expression accompany antigen-induced murine T-cell activation. Proc. Natl. Acad. Sci. U S A *86*, 6734–6738. https://doi.org/10.1073/pnas.86.17.6734.

Byth, K.F., Conroy, L.A., Howlett, S., Smith, A.J., May, J., Alexander, D.R., and Holmes, N. (1996). CD45-null transgenic mice reveal a positive regulatory role for CD45 in early thymocyte development, in the selection of CD4+CD8+ thymocytes, and B cell maturation. J. Exp. Med. *183*, 1707–1718. https://doi.org/10.1084/jem.183.4.1707.

Cabañas, C., Yáñez-Mó, M., and van Spriel, A.B. (2019). Editorial: functional relevance of tetraspanins in the immune system. Front. Immunol. *10*, 1714. https://doi.org/10.3389/fimmu.2019.01714.

Cairo, C.W., Das, R., Albohy, A., Baca, Q.J., Pradhan, D., Morrow, J.S., Coombs, D., and Golan, D.E. (2010). Dynamic regulation of CD45 lateral mobility by the spectrin-ankyrin cytoskeleton of T cells. J. Biol. Chem. *285*, 11392–11401. https://doi.org/10.1074/jbc.m109.075648.

Carbone, C.B., Kern, N., Fernandes, R.A., Hui, E., Su, X., Garcia, K.C., and Vale, R.D. (2017). In vitro reconstitution of T cell receptor-mediated segregation of the CD45 phosphatase. Proc. Natl. Acad. Sci. U S A *114*, E9338–E9345. https://doi.org/10.1073/pnas.1710358114.

Carmo, A.M., and Wright, M.D. (1995). Association of the transmembrane 4 superfamily molecule CD53 with a tyrosine phosphatase activity. Eur. J. Immunol. *25*, 2090–2095. https://doi.org/10.1002/eji.1830250743.

Chang, V.T., Fernandes, R.A., Ganzinger, K.A., Lee, S.F., Siebold, C., McColl, J., Jönsson, P., Palayret, M., Harlos, K., Coles, C.H., et al. (2016). Initiation of T cell signaling by CD45 segregation at "close contacts. Nat. Immunol. *17*, 574–582. https://doi.org/10.1038/ni.3392.

Charrin, S., Jouannet, S., Boucheix, C., and Rubinstein, E. (2014). Tetraspanins at a glance. J. Cell Sci. *127*, 3641–3648. https://doi.org/10.1242/jcs.154906.

Chen, I.-J., Chen, H.-L., and Demetriou, M. (2007). Lateral compartmentalization of T cell receptor versus CD45 by galectin-N-glycan binding and microfilaments coordinate basal and activation signaling. J. Biol. Chem. *282*, 35361–35372. https://doi.org/10.1074/jbc.m706923200.

Chui, D., Ong, C.J., Johnson, P., Teh, H.S., and Marth, J.D. (1994). Specific CD45 isoforms differentially regulate T cell receptor signaling. EMBO J. *13*, 798–807. https://doi.org/10.1002/j.1460-2075.1994.tb06322.x.

Clement, L.T. (1992). Isoforms of the CD45 common leukocyte antigen family: markers for human T-cell differentiation. J. Clin. Immunol. *12*, 1–10. https://doi.org/10.1007/bf00918266.

Cordoba, S.-P., Choudhuri, K., Zhang, H., Bridge, M., Basat, A.B., Dustin, M.L., and van der Merwe, P.A. (2013). The large ectodomains of CD45 and CD148 regulate their segregation from and inhibition of ligated T-cell receptor. Blood *121*, 4295–4302. https://doi.org/10.1182/blood-2012-07-442251.

Courtney, A.H., Shvets, A.A., Lu, W., Griffante, G., Mollenauer, M., Horkova, V., Lo, W.-L., Yu, S., Stepanek, O., Chakraborty, A.K., et al. (2019). CD45 functions as a signaling gatekeeper in T cells. Sci. Signal. *12*, eaaw8151. https://doi.org/10.1126/scisignal.aaw8151.

Craig, W., Poppema, S., Little, M.-T., Dragowska, W., and Lansdorp, P.M. (1994). CD45 isoform expression on human haemopoietic cells at different stages of development. Br. J. Haematol. *88*, 24–30. https://doi.org/10.1111/j.1365-2141.1994.tb04972.x.

Dawes, R., Petrova, S., Liu, Z., Wraith, D., Beverley, P.C.L., and Tchilian, E.Z. (2006). Combinations of CD45 isoforms are crucial for immune function and disease. J. Immunol. *176*, 3417–3425. https://doi.org/10.4049/jimmunol.176.6.3417.

Demaria, M.C., Yeung, L., Peeters, R., Wee, J.L., Mihaljcic, M., Jones, E.L., Nasa, Z., Alderuccio, F., Hall, P., Smith, B.C., et al. (2020). Tetraspanin CD53 promotes lymphocyte recirculation by stabilizing L-selectin surface expression. iScience *23*, 101104. https://doi.org/10.1016/j.isci.2020.101104.

van Deventer, S., Arp, A.B., and van Spriel, A.B. (2021). Dynamic plasma membrane organization: a complex symphony. Trends Cell Biol. *31*, 119–129. https://doi.org/10.1016/j.tcb.2020.11.004.

Van Deventer, S.J., Dunlock, V.-M.E., and Van Spriel, A.B. (2017). Molecular interactions shaping the tetraspanin web. Biochem. Soc. Trans. *45*, 741–750. https://doi.org/10.1042/bst20160284.

Dornan, S., Sebestyen, Z., Gamble, J., Nagy, P., Bodnar, A., Alldridge, L., Doe, S., Holmes, N., Goff, L.K., Beverley, P., et al. (2002). Differential association of CD45 isoforms with CD4 and CD8 regulates the actions of specific pools of p56lck tyrosine kinase in T cell antigen receptor signal transduction. J. Biol. Chem. *277*, 1912–1918. https://doi.org/10.1074/jbc.m108386200.

van den Dries, K., van Helden, S.F.G., Riet, J., Cambi, A., Figdor, C.G., Diez-Ahedo, R., Manzo, C., Oud, M.M., van Leeuwen, F.N., et al. (2012). Geometry sensing by dendritic cells dictates spatial organization and PGE2-induced dissolution of podosomes. Cell. Mol. Life Sci. *69*, 1889–1901. https://doi.org/10.1007/s00018-011-0908-y.

Dunlock, V.E. (2020). Tetraspanin CD53: an overlooked regulator of immune cell function. Med. Microbiol. Immunol. *209*, 545–552. https://doi.org/10.1007/s00430-020-00677-z.

Fabre, J.W., and Williams, A.F. (1977). Quantitative serological analysis of a rabbit anti-rat lymphocyte serum and preliminary biochemical characterisation of the major antigen recognised. Transplantation *23*, 349–359. https://doi.org/10.1097/00007890-197704000-00009.

Furlan, G., Minowa, T., Hanagata, N., Kataoka-Hamai, C., and Kaizuka, Y. (2014). Phosphatase CD45 both positively and negatively regulates T cell

receptor phosphorylation in reconstituted membrane protein clusters. J. Biol. Chem. *289*, 28514–28525. https://doi.org/10.1074/jbc.m114.574319.

Furukawa, T., Itoh, M., Krueger, N.X., Streuli, M., and Saito, H. (1994). Specific interaction of the CD45 protein-tyrosine phosphatase with tyrosine-phosphorylated CD3 zeta chain. Proc. Natl. Acad. Sci. U S A *91*, 10928–10932. https://doi.org/10.1073/pnas.91.23.10928.

Gartlan, K.H., Wee, J.L., Demaria, M.C., Nastovska, R., Chang, T.M., Jones, E.L., Apostolopoulos, V., Pietersz, G.A., Hickey, M.J., van Spriel, A.B., et al. (2013). Tetraspanin CD37 contributes to the initiation of cellular immunity by promoting dendritic cell migration. Eur. J. Immunol. *43*, 1208–1219. https://doi.org/10.1002/eji.201242730.

Gonsky, R., Deem, R.L., Lee, D.H., Chen, A., and Targan, S.R. (1999). CD28 costimulation augments IL-2 secretion of activated lamina propria T cells by increasing mRNA stability without enhancing IL-2 gene transactivation. J. Immunol. *162*, 6621–6629.

Griesbeck, O., Baird, G.S., Campbell, R.E., Zacharias, D.A., and Tsien, R.Y. (2001). Reducing the environmental sensitivity of yellow fluorescent protein. J. Biol. Chem. *276*, 29188–29194. https://doi.org/10.1074/jbc.m102815200.

He, H.-T., and Bongrand, P. (2012). Membrane dynamics shape TCR-generated signaling. Front. Immunol. *3*, 90. https://doi.org/10.3389/fimmu.2012.00090.

Hsu, P.D., Scott, D.A., Weinstein, J.A., Ran, F.A., Konermann, S., Agarwala, V., Li, Y., Fine, E.J., Wu, X., Shalem, O., et al. (2013). DNA targeting specificity of RNA-guided Cas9 nucleases. Nat. Biotechnol. *31*, 827–832. https://doi.org/10.1038/nbt.2647.

Jin, M., Shi, N., Wang, M., Shi, C., Lu, S., Chang, Q., Sha, S., Lin, Y., Chen, Y., Zhou, H., et al. (2020). CD45: a critical regulator in immune cells to predict severe and non-severe COVID-19 patients. Aging (Albany. NY) *12*, 19867–19879.

Jung, Y., Wen, L., Altman, A., and Ley, K. (2021). CD45 pre-exclusion from the tips of T cell microvilli prior to antigen recognition. Nat. Commun. *12*, 3872. https://doi.org/10.1038/s41467-021-23792-8.

Kishihara, K., Penninger, J., Wallace, V.A., Kündig, T.M., Kawal, K., Wakeham, A., Timms, E., Pfeffer, K., Ohashi, P.S., Thomas, M.L., et al. (1993). Normal B lymphocyte development but impaired T cell maturation in CD45-Exon6 protein tyrosine phosphatase-deficient mice. Cell *74*, 143–156. https://doi.org/10.1016/0092-8674(93)90302-7.

Koulouras, G., Panagopoulos, A., Rapsomaniki, M.A., Giakoumakis, N.N., Taraviras, S., and Lygerou, Z. (2018). EasyFRAP-web: a web-based tool for the analysis of fluorescence recovery after photobleaching data. Nucleic Acids Res. *46*, W467–W472. https://doi.org/10.1093/nar/gky508.

Kremers, G.-J., Goedhart, J., van den Heuvel, D.J., Gerritsen, H.C., and Gadella, T.W.J. (2007). Improved green and blue fluorescent proteins for expression in bacteria and mammalian cells. Biochemistry *46*, 3775–3783. https://doi.org/10.1021/bi0622874.

Krummey, S.M., Morris, A.B., Jacobs, J.R., McGuire, D.J., Ando, S., Tong, K.P., Zhang, W., Robertson, J., Guasch, S.A., Araki, K., et al. (2020). CD45RB status of CD8(+) T cell memory defines T cell receptor affinity and persistence. Cell Rep. *30*, 1282–1291.e5. https://doi.org/10.1016/j.celrep.2020.01.016.

Kung, C., Pingel, J.T., Heikinheimo, M., Klemola, T., Varkila, K., Yoo, L.I., Vuopala, K., Poyhonen, M., Uhari, M., Rogers, M., et al. (2000). Mutations in the tyrosine phosphatase CD45 gene in a child with severe combined immunodeficiency disease. Nat. Med. *6*, 343–345. https://doi.org/10.1038/73208.

Lapalombella, R., Yeh, Y.-Y., Wang, L., Ramanunni, A., Rafiq, S., Jha, S., Staubli, J., Lucas, D.M., Mani, R., Herman, S.E.M., et al. (2012). Tetraspanin CD37 directly mediates transduction of survival and apoptotic signals. Cancer Cell *21*, 694–708. https://doi.org/10.1016/j.ccr.2012.03.040.

Levy, S., and Shoham, T. (2005). The tetraspanin web modulates immune-signalling complexes. Nat. Rev. Immunol. *5*, 136–148. https://doi.org/10.1038/nri1548.

Majeti, R., Xu, Z., Parslow, T.G., Olson, J.L., Daikh, D.I., Killeen, N., and Weiss, A. (2000). An inactivating point mutation in the inhibitory wedge of CD45 causes lymphoproliferation and autoimmunity. Cell *103*, 1059–1070. https://doi.org/10.1016/s0092-8674(00)00209-9.

McNeill, L., Cassady, R.L., Sarkardei, S., Cooper, J.C., Morgan, G., and Alexander, D.R. (2004). CD45 isoforms in T cell signalling and development. Immunol. Lett. *92*, 125–134. https://doi.org/10.1016/j.imlet.2003.10.018.

McNeill, L., Salmond, R.J., Cooper, J.C., Carret, C.K., Cassady-Cain, R.L., Roche-Molina, M., Tandon, P., Holmes, N., and Alexander, D.R. (2007). The differential regulation of lck kinase phosphorylation sites by CD45 is critical for T cell receptor signaling responses. Immunity *27*, 425–437. https://doi.org/10.1016/j.immuni.2007.07.015.

Mollinedo, F., Fontán, G., Barasoain, I., and Lazo, P.A. (1997). Recurrent infectious diseases in human CD53 deficiency. Clin. Diagn. Lab. Immunol. *4*, 229–231. https://doi.org/10.1128/cdli.4.2.229-231.1997.

Nika, K., Soldani, C., Salek, M., Paster, W., Gray, A., Etzensperger, R., Fugger, L., Polzella, P., Cerundolo, V., Dushek, O., et al. (2010). Constitutively active Lck kinase in T cells drives antigen receptor signal transduction. Immunity *32*, 766–777. https://doi.org/10.1016/j.immuni.2010.05.011.

Novak, T.J., Farber, D., Leitenberg, D., Hong, S.C., Johnson, P., and Bottomly, K. (1994). Isoforms of the transmembrane tyrosine phosphatase CD45 differentially affect T cell recognition. Immunity *1*, 109–119. https://doi.org/10.1016/1074-7613(94)90104-x.

Nyakeriga, A.M., Garg, H., and Joshi, A. (2012). TCR-induced T cell activation leads to simultaneous phosphorylation at Y505 and Y394 of p56(lck) residues. Cytometry *81A*, 797–805. https://doi.org/10.1002/cyto.a.22070.

Oka, S., Mori, N., Matsuyama, S., Takamori, Y., and Kubo, K. (2000). Presence of B220 within thymocytes and its expression on the cell surface during apoptosis. Immunology *100*, 417–423. https://doi.org/10.1046/j.1365-2567.2000.00063.x.

Palacios, E.H., and Weiss, A. (2004). Function of the src-family kinases, lck and Fyn, in T-cell development and activation. Oncogene *23*, 7990–8000. https://doi.org/10.1038/sj.onc.1208074.

Pingel, J.T., and Thomas, M.L. (1989). Evidence that the leukocyte-common antigen is required for antigen-induced T lymphocyte proliferation. Cell *58*, 1055–1065. https://doi.org/10.1016/0092-8674(89)90504-7.

Plunkett, T., Graham, R., Correa, I., Sewell, R., Miles, D., Burchell, J., and Taylor-Papadimitriou, J. (2004). Protection against MUC1 expressing mouse tumours by intra-muscular injection of MUC1 cDNA requires functional CD8+ and CD4+ T cells but does not require the MUC1 tandem repeat domain. Int. J. Cancer *109*, 691–697. https://doi.org/10.1002/ijc.20040.

Pokoyski, C., Lienen, T., Rother, S., Schock, E., Plege-Fleck, A., Geffers, R., Schwinzer, R., and Plege-Fleck, A. (2015). Overexpression of CD45RA isoforms in carriers of the C77G mutation leads to hyporeactivity of CD4+CD25highFoxp3+ regulatory T cells. Gene Immun. *16*, 519–527. https://doi.org/10.1038/gene.2015.39.

Porcu, M., Kleppe, M., Gianfelici, V., Geerdens, E., De Keersmaecker, K., Tartaglia, M., Foà, R., Soulier, J., Cauwelier, B., Uyttebroeck, A., et al. (2012). Mutation of the receptor tyrosine phosphatase PTPRC (CD45) in T-cell acute lymphoblastic leukemia. Blood *119*, 4476–4479. https://doi.org/10.1182/blood-2011-09-379958.

Pradhan, D., and Morrow, J.S. (2002). The spectrin-ankyrin skeleton controls CD45 surface display and interleukin-2 production. Immunity *17*, 303–315. https://doi.org/10.1016/s1074-7613(02)00396-5.

Pulido, R., and Sánchez-Madrid, F. (1992). Glycosylation of CD45: carbohydrate processing through Golgi apparatus is required for cell surface expression and protein stability. Eur. J. Immunol. *22*, 463–468. https://doi.org/10.1002/eji.1830220226.

Puls, K.L., Hogquist, K.A., Reilly, N., and Wright, M.D. (2002). CD53, a thymocyte selection marker whose induction requires a lower affinity TCR-MHC interaction than CD69, but is up-regulated with slower kinetics. Int. Immunol. *14*, 249–258. https://doi.org/10.1093/intimm/14.3.249.

Pyzocha, N.K., Ran, F.A., Hsu, P.D., and Zhang, F. (2014). RNA-guided genome editing of mammalian cells. Methods Mol. Biol. *1114*, 269–277.

Razvag, Y., Neve-Oz, Y., Sajman, J., Reches, M., and Sherman, E. (2018). Nanoscale kinetic segregation of TCR and CD45 in engaged microvilli facilitates early T cell activation. Nat. Commun. *9*, 732. https://doi.org/10.1038/s41467-018-03127-w.

Rip, J., de Bruijn, M.J.W., Kaptein, A., Hendriks, R.W., and Corneth, O.B.J. (2020). Phosphoflow protocol for signaling studies in human and murine B cell subpopulations. J. Immunol. *204*, 2852–2863. https://doi.org/10.4049/jimmunol.1901117.

Roberts, J.L., Buckley, R.H., Luo, B., Pei, J., Lapidus, A., Peri, S., Wei, Q., Shin, J., Parrott, R.E., Dunbrack, R.L., et al. (2012). CD45-deficient severe combined immunodeficiency caused by uniparental disomy. Proc. Natl. Acad. Sci. U S A *109*, 10456–10461. https://doi.org/10.1073/pnas.1202249109.

Seu, L., Tidwell, C., Timares, L., Duverger, A., Wagner, F.H., Goepfert, P.A., Westfall, A.O., Sabbaj, S., and Kutsch, O. (2017). CD151 expression is associated with a hyperproliferative T cell phenotype. J. Immunol. *199*, 3336–3347. https://doi.org/10.4049/jimmunol.1700648.

Shanafelt, M.C., Yssel, H., Soderberg, C., Steinman, L., Adelman, D.C., Peltz, G., and Lahesmaa, R. (1996). CD45 isoforms on human CD4+ T-cell subsets. J. Allergy Clin. Immunol. *98*, 433–440. https://doi.org/10.1016/s0091-6749(96)70168-9.

Shaner, N.C., Campbell, R.E., Steinbach, P.A., Giepmans, B.N.G., Palmer, A.E., and Tsien, R.Y. (2004). Improved monomeric red, orange and yellow fluorescent proteins derived from Discosoma sp. red fluorescent protein. Nat. Biotechnol. *22*, 1567–1572. https://doi.org/10.1038/nbt1037.

van Spriel, A.B., Puls, K.L., Sofi, M., Pouniotis, D., Hochrein, H., Orinska, Z., Knobeloch, K.-P., Plebanski, M., and Wright, M.D. (2004). A regulatory role for CD37 in T cell proliferation. J. Immunol. *172*, 2953–2961. https://doi.org/10.4049/jimmunol.172.5.2953.

Stanford, S.M., Panchal, R.G., Walker, L.M., Wu, D.J., Falk, M.D., Mitra, S., Damle, S.S., Ruble, D., Kaltcheva, T., Zhang, S., et al. (2012). High-throughput screen using a single-cell tyrosine phosphatase assay reveals biologically active inhibitors of tyrosine phosphatase CD45. Proc. Natl. Acad. Sci. U S A. *109*, 13972–13977. https://doi.org/10.1073/pnas.1205028109.

Szodoray, P., Stanford, S.M., Molberg, Ø., Munthe, L.A., Bottini, N., and Nakken, B. (2016). T-helper signals restore B-cell receptor signaling in autoreactive anergic B cells by upregulating CD45 phosphatase activity. J. Allergy Clin. Immunol. *138*, 839–851.e8. https://doi.org/10.1016/j.jaci.2016.01.035.

Tackenberg, B., Nitschke, M., Willcox, N., Ziegler, A., Nessler, S., Schumm, F., Oertel, W.H., Hemmer, B., and Sommer, N. (2003). CD45 isoform expression in autoimmune myasthenia gravis. Autoimmunity *36*, 117–121. https://doi.org/10.1080/0891693031000084369.

Tarrant, J.M., Groom, J., Metcalf, D., Li, R., Borobokas, B., Wright, M.D., Tarlinton, D., and Robb, L. (2002). The absence of Tssc6, a member of the tetraspanin superfamily, does not affect lymphoid development but enhances in vitro T-cell proliferative responses. Mol. Cell Biol. *22*, 5006–5018. https://doi.org/10.1128/mcb.22.14.5006-5018.2002.

Tchilian, E.Z., and Beverley, P.C.L. (2006). Altered CD45 expression and disease. Trends Immunol. *27*, 146–153. https://doi.org/10.1016/j.it.2006.01.001.

Tchilian, E.Z., Wallace, D.L., Wells, R.S., Flower, D.R., Morgan, G., and Beverley, P.C.L. (2001). A deletion in the gene encoding the CD45 antigen in a patient with SCID. J. Immunol. *166*, 1308–1313. https://doi.org/10.4049/jimmunol.166.2.1308.

Termini, C.M., and Gillette, J.M. (2017). Tetraspanins function as regulators of cellular signaling. Front. Cell Dev. Biol. *5*, 34. https://doi.org/10.3389/fcell.2017.00034.

Tomlinson, M.G., Hanke, T., Hughes, D.A., Barclay, A.N., Scholl, E., Hünig, T., and Wright, M.D. (1995). Characterization of mouse CD53: epitope mapping, cellular distribution and induction by T cell receptor engagement during repertoire selection. Eur. J. Immunol. *25*, 2201–2205. https://doi.org/10.1002/eji.1830250813.

Trowbridge, I.S. (1978). Interspecies spleen-myeloma hybrid producing monoclonal antibodies against mouse lymphocyte surface glycoprotein, T200. J. Exp. Med. *148*, 313–323. https://doi.org/10.1084/jem.148.1.313.

Umlauf, S.W., Beverly, B., Lantz, O., and Schwartz, R.H. (1995). Regulation of interleukin 2 gene expression by CD28 costimulation in mouse T-cell clones: both nuclear and cytoplasmic RNAs are regulated with complex kinetics. Mol. Cell Biol. *15*, 3197–3205. https://doi.org/10.1128/mcb.15.6.3197.

Vogel, A., Strassburg, C.P., Manns, M.P., and Vogel, A. (2003). 77 C/G mutation in the tyrosine phosphatase CD45 gene and autoimmune hepatitis: evidence for a genetic link. Gene Immun. *4*, 79–81. https://doi.org/10.1038/sj.gene.6363918.

Vremec, D., Pooley, J., Hochrein, H., Wu, L., and Shortman, K. (2000). CD4 and CD8 expression by dendritic cell subtypes in mouse thymus and spleen. J. Immunol. *164*, 2978–2986. https://doi.org/10.4049/jimmunol.164.6.2978.

Wei, Q., Brzostek, J., Sankaran, S., Casas, J., Hew, L.S.-Q., Yap, J., Zhao, X., Wojciech, L., and Gascoigne, N.R.J. (2020). Lck bound to coreceptor is less active than free Lck. Proc. Natl. Acad. Sci. U. S. A. *117*, 15809–15817. https://doi.org/10.1073/pnas.1913334117.

Xu, Z., and Weiss, A. (2002). Negative regulation of CD45 by differential homodimerization of the alternatively spliced isoforms. Nat. Immunol. *3*, 764–771. https://doi.org/10.1038/ni822.

Yáñez-Mó, M., Barreiro, O., Gordon-Alonso, M., Sala-Valdés, M., and Sánchez-Madrid, F. (2009). Tetraspanin-enriched microdomains: a functional unit in cell plasma membranes. Trends Cell Biol. *19*, 434–446. https://doi.org/10.1016/j.tcb.2009.06.004.

Yeung, L., Anderson, J.M.L., Wee, J.L., Demaria, M.C., Finsterbusch, M., Liu, Y.S., Hall, P., Smith, B.C., Dankers, W., Elgass, K.D., et al. (2020). Leukocyte tetraspanin CD53 restrains α3 integrin mobilization and facilitates cytoskeletal remodeling and transmigration in mice. J. Immunol. *205*, 521–532. https://doi.org/10.4049/jimmunol.1901054.

Zhang, M., Moran, M., Round, J., Low, T.A., Patel, V.P., Tomassian, T., Hernandez, J.D., and Miceli, M.C. (2005). CD45 signals outside of lipid rafts to promote ERK activation, synaptic raft clustering, and IL-2 production. J. Immunol. *174*, 1479–1490. https://doi.org/10.4049/jimmunol.174.3.1479.

Zikherman, J., Jenne, C., Watson, S., Doan, K., Raschke, W., Goodnow, C.C., and Weiss, A. (2010). CD45-Csk phosphatase-kinase titration uncouples basal and inducible T cell receptor signaling during thymic development. Immunity *32*, 342–354. https://doi.org/10.1016/j.immuni.2010.03.006.

Zuidscherwoude, M., Dunlock, V.-M.E., Van Den Bogaart, G., Van Deventer, S.J., Van Der Schaaf, A., Van Oostrum, J., Goedhart, J., In't Hout, J., Hämmerling, G.J., Tanaka, S., et al. (2017). Tetraspanin microdomains control localized protein kinase C signaling in B cells. Sci. Signal. *10*, eaag2755. https://doi.org/10.1126/scisignal.aag2755.

STAR★METHODS

KEY RESOURCES TABLE

REAGENT or RESOURCE	SOURCE	IDENTIFIER
Antibodies		
Mouse Monoclonal anti-human CD53	Biorad	Clone: MEM-53 Cat# MCA723G
Mouse Monoclonal anti-human CD53	Diaclone	Clone: TS53 Cat# 857.760.000
Mouse Monoclonal anti-human CD53 Alexa-488	Novus Biologicals	Clone: MEM-53 Cat#NB500-393AF488
Mouse Monoclonal anti-human CD3	BioXcell	Clone: OKT-3 Cat# BE0001-2
Mouse Monoclonal anti-human CD28	BioXcell	Clone: 9.3 Cat# BE0248
Monoclonal REAfinity anti-human CD45	Miltenyi	Clone: REA747 Cat# 130-122-311
Mouse Monoclonal anti-human CD45RA PE	Biolegend	Clone: HI30 Cat# 304002
Mouse Monoclonal anti-human CD45RO APC	BD Pharmingen	Clone: UCHL1 Cat# 555493
Mouse Monoclonal anti-human CD45	Beckman Coulter	Clone: ALB12 Cat# IM647
Mouse Monoclonal anti-human CD45RA	Novus Biologicals	Clone: MEM-56 Cat# NB500-329
Mouse Monoclonal anti-human CD45RO	Thermo Fisher Scientific	Clone: UCHL1 Cat# UM800136
Mouse Monoclonal anti-human CD45	Abcam	Clone: MEM-28 Cat# ab8216
Rabbit Polyclonal anti-human CD45	Abcam	Cat# ab10558
Mouse Monoclonal anti-human CD3 PE	BD Pharmingen	Clone: HIT3a Cat# 561803
Mouse Monoclonal anti-human CD4 APC	Biolegend	Clone: RPA-T4 Cat# 300502
Mouse Monoclonal anti-human CD4 PerCP	Biolegend	Clone: RPA-T4 Cat# 300528
Mouse Monoclonal anti-human CD8 FITC	BD Pharmingen	Clone: RPA-T8 Cat# 561948
Mouse Monoclonal anti-human CD8 APC	BD Pharmingen	Clone: RPA-T8 Cat# 555369
Mouse Monoclonal anti-human CD25 PE	BD Pharmingen	Clone: M-A251 Cat# 557138
Mouse Monoclonal anti-human CD69 PerCP	BD Pharmingen	Clone: L78 Cat# 340368
Mouse Monoclonal anti-human CD151	Biorad	Clone: 11G5a Cat# MCA1856
Rat monoclonal anti-mouse CD3	BioXcell	Clone: 17A2 Cat# BE0002
Syrian Hamster monoclonal anti-mouse CD28	BioXcell	Clone: 37.51 Cat# BE0015-1
Syrian Hamster monoclonal anti-mouse CD28	BD Pharmingen	Clone: 37.51 Cat# 557393

(*Continued on next page*)

Continued

REAGENT or RESOURCE	SOURCE	IDENTIFIER
Armenian Hamster monoclonal anti-mouse CD3e	Biolegend	Clone: 145-2C11
Rat monoclonal anti-mouse CD3	Biolegend	Clone: 17A2 Cat# 100238
Rat Monoclonal anti-mouse CD4 FITC	Biolegend	Clone: RM4-5 Cat# 100510
Rat Monoclonal anti-mouse CD4 PerCP	Biolegend	Clone: RM4-5 Cat# 100538
Rat Monoclonal anti-mouse CD4 APC	Biolegend	Clone: RM4-5 Cat# 100516
Rat Monoclonal anti-mouse CD8 PE	BD Pharmingen	Clone: 53-6.7 Cat# 553032
Rat Monoclonal anti-mouse CD8 PE-Cy7	Biolegend	Clone: 53-6.7 Cat# 100722
Rat Monoclonal anti-mouse CD8 PerCP	BD Pharmingen	Clone: 53-6.7 Cat# 553036
Rat Monoclonal anti-mouse CD8 FITC	BD Pharmingen	Clone: 53-6.7 Cat# 553031
Rat Monoclonal anti-mouse CD25 APC	eBioscience/Thermo Fisher	Clone: PC61.5 Cat# 17-0251-82
Armenian Hamster Monoclonal anti-mouse CD69 PE	BD Pharmingen	Clone: H1.2F3 Cat# 553237
Rat Monoclonal anti-mouse CD44 PECy7	Biolegend	Clone: IM7 Cat# 103030
Rat Monoclonal anti-mouse CD62L BV510	Biolegend	Clone: MEL-14 Cat# 104441
Rat Monoclonal anti-mouse IL-2 PE	Biolegend	Clone: JES6-5H4 Cat# 503808
Rat Monoclonal anti-mouse IL-2	Biolegend	Clone: JES6-5H4 Cat# 503802
Rat Monoclonal anti-mouse IL-2 Biotin	Biolegend	Clone: JES6-5H4 Cat# 503804
Rat Monoclonal anti-mouse Siglec H Alexa-647	Biolegend	Clone: 551 Cat# 129608
Rat Monoclonal anti-mouse CD11b	Biolegend	Clone: M1/70 Cat# 101208
Rat Monoclonal anti-mouse CD45 Alexa-647	Biolegend	Clone: RA3-6B2 Cat# 103226
Rat Monoclonal anti-mouse CD45 Alexa-700	eBioscience	Clone: RA3-6B2 Cat# 56-0452-82
Rat Monoclonal anti-mouse CD45 FITC	Biolegend	Clone: RA3-6B2 Cat# 103206
Hamster Monoclonal anti-mouse CD11c PECy7	BD Pharmingen	Clone: HL3 Cat# 561022
Hamster Monoclonal anti-mouse CD11c APC	BD Pharmingen	Clone: HL3 Cat# 561119
Rat Monoclonal anti-mouse CD172 APC	BD Pharmingen	Clone: p84 Cat# 560106
Mouse Monoclonal anti-mouse MHCI H-2Kb/H-2Db PE	Biolegend	Clone: 28-86 Cat# 114608
Rat Monoclonal anti-mouse MHCII I-A/I-E PE	eBioscience/Thermo Fisher	Clone: M5/114.15.2 Cat# 12-5321-82

(*Continued on next page*)

Continued

REAGENT or RESOURCE	SOURCE	IDENTIFIER
Rat Monoclonal anti-mouse MHCII I-A/I-E PerCP	eBioscience/Thermo Fisher	Clone: M5/114.15.2 Cat# 46-5321-82
Rabbit Monoclonal mix anti-mouse Phospho-Tyrosine	Cell Signaling	Cat# 8954S
Rat Monoclonal anti-mouse L-selectin/ CD62L BV510	Biolegend	Clone: MEL-14 Cat# 104441
Rat Monoclonal anti-mouse CD44	Biolegend	Clone: IM7 Cat# 103030
Goat anti-Armenian hamster IgG Biotin	Biolegend	Cat# 405501
Rabbit Polyclonal pLck (Y394) PE	Merck	Cat# SAB4300118
Mouse Monoclonal anti-mouse pCD3z (Y142) PE	Invitrogen	Clone:3ZBR4S Cat# 12-2478-42
Goat Polyclonal anti-rabbit IgG PE	Invitrogen	Cat# P-2771MP
Mouse Monoclonal anti-Human CD9	Diaclone	Cat# 857.750.000
Mouse Monoclonal anti-Human CD81	Diaclone	Cat# 857.780.000
Rabbit Monoclonal anti-Human CD45	Cell Signaling Technologies	Clone: D9M8I Cat# 13917
Donkey anti-Rabbit IgG IRDye 800CW	Li-Cor	Cat# 926-32213
Clone 4/LCK Y505	BD Biosciences	Cat# 558577
Mouse anti-tyrosine 4G10	Millipore	Cat# 05-321
Rabbit anti-Phospho-Tyrosine (P-Tyr-1000)	Cell signaling	Cat# 8954S
Rabbit anti-CD3 zeta (phospho Y142) [EP265(2)Y]	Abcam	Cat# ab68235
Rat anti-Tubulin	Novus Biologicals	Cat# NB100-1639
Biological samples		
Human Peripheral Blood (buffy coats)	Sanquin Blood Bank	N/A
Chemicals, peptides, and recombinant proteins		
pCap-SP1 CD45 activity Probe	Stanford et al., 2012; Szodoray et al., 2016	N/A
NP-Keyhole limpet haemocyanin (KLH)	Biosearch Technologies	Cat# N-5060-5
Imject Alum adjuvant	Sigma	Cat# 77161
DNase I endonuclease	New England Biolabs	Cat# M0303L
Collagenase type III	Worthington	Cat# LS004182
Recombinant Flt3L	eBioscience/Thermo Fisher	Cat# 14-8001-80
Endograde Chicken Ovalbumin	Hyglos GmbH	Cat# 321000
Critical commercial assays		
CellTrace Violet Proliferation Kit	Thermo Fisher Scientific	Cat# C34557
CellTrace CFSE Proliferation Kit	Thermo Fisher Scientific	Cat# C34554
Fixable viability dye eFluor 506	Invitrogen	Cat# 65-0866-14
Human IL-2 ELISA Kit	Thermo Fisher Scientific	Cat# EH2IL25
Murine IL-2 ELISA Kit	Thermo Fisher Scientific	Cat# BMS601TEN
Pan T cell Isolation Kit II, Mouse	Miltenyi Biotec	Cat# 130-095-130
CD3e Microbead Kit, Mouse	Miltenyi Biotec	Cat# 130-094-973
Pan T cell Isolation Kit, Human	Miltenyi Biotec	Cat# 130-096-535
BD Cytofix/Cytoperm Kit	BD Pharmingen	Cat# 554714
Duolink In Situ PLA Orange Kit	Sigma	Cat# DUO92007
Neon™ Transfection System 100 μL Kit	Thermo Fisher Scientific	Cat# MPK10096
Deposited data		
Immunoprecipitation Data	Dr. E. Rubinstein (Inserm, Paris)	N/A

(*Continued on next page*)

Continued

REAGENT or RESOURCE	SOURCE	IDENTIFIER
Experimental models: Cell lines		
Human CCRF-CEM T cell	ATCC	Cat# CRM-CCL-119
Human Jurkat T cell	ATCC	Cat# CRL-2899
Human Raji B cell	ATCC	Cat# CCL-86
RMA-Muc1 Tumor Line	Gartlan et al., 2013	N/A
B16-OVA Tumor Line	Gartlan et al., 2013	N/A
Experimental models: Organisms/strains		
Cd53$^{-/-}$ Mouse Strain	Zuidscherwoude et al., 2017	N/A
C57Bl/6J WT (*Cd53*$^{+/+}$) Mouse Strain	Jackson Lab backcrossed into *Cd53*$^{-/-}$ strain to create littermate line	Stock No: 000664
OT-I Mouse Strain	Charles River	Strain Code: 642
OT-II Mouse Strain	Charles River	Strain code: 643
Oligonucleotides		
CD53 CRISPR RNA guide 1: TGATAGAGCCCATGCAGCCCAG	N/A	N/A
CD53 CRISPR RNA guide 2: GTGAGTCCTTACAGCAGATGTGG	N/A	N/A
Recombinant DNA		
hCD45RO-sGFP2	Subcloned Genscript construct (Kremers et al., 2007)	N/A
hCD45-mCherry	Subcloned Genscript construct (Shaner et al., 2004)	N/A
hCD45RA-sGFP2	Subcloned Genscript construct (Kremers et al., 2007)	N/A
hCD45RA-mCherry	Subcloned Genscript construct (Shaner et al., 2004)	N/A
sGFP2-hCD53	Subcloned cDNA (NM_000560, Thermo Scientific) (Kremers et al., 2007)	N/A
mCitrine-hCD53	Subcloned cDNA (NM_000560, Thermo Scientific) (Griesbeck et al., 2001)	N/A
sGFP2-hCD37	(Lapalombella et al., 2012)	N/A
hPKC θ-mCherry	Subcloned Genscript construct (Shaner et al., 2004)	N/A
hCD45RA-sGFP2	Subcloned Genscript construct (Kremers et al., 2007)	N/A
Software and algorithms		
Fiji image analysis Software	Fiji	N/A
FlowJo v9 Software	FlowJo	N/A
OriginPro 8 Software	OriginLab	N/A
Image Studio Lite Software	Licor	N/A
GraphPad Prism 5 Software	Prism	N/A
Leica LasX Software	Leica	N/A
Zeiss Zen Software	Zeiss	N/A
Proteome Discoverer 1.4 Software	Thermo Fisher	N/A
EasyFrap Software	Koulouras et al., 2018	N/A

RESOURCE AVAILABILITY

Lead contact

Further information and requests for resources and reagents should be directed to and will be fulfilled by the lead contact, Prof. Annemiek van Spriel (Annemiek.vanSpriel@radboudumc.nl).

Materials availability

Plasmids, cell lines and mouse lines generated in this study are available from the lead contact upon request.

Data and code availability

All data reported in this paper will be shared by the lead contact upon request. This paper does not report original code. Any additional information required to reanalyze the data reported in this paper is available from the lead contact upon request.

EXPERIMENTAL MODEL AND SUBJECT DETAILS

Animals

Generation of *Cd53*$^{-/-}$ mice has been described previously (Zuidscherwoude et al., 2017). *Cd53*$^{-/-}$ mice and sex- and aged-matched C57Bl/6J WT (*Cd53*+/+) littermate mice were bred at the Central Animal Laboratory, Nijmegen (the Netherlands). Both female and male age-matched mice were used in replicate experiments. OT-I and OT-II mice were obtained from Charles River. Mice were housed in top-filter cages and fed a standard diet with freely available water and food and used at 6 to 18 weeks of age. All murine studies complied with European legislation and were approved by the local animal ethical committee for the care and use of animals with related codes of practice.

Cells

CEM, Jurkat and Raji cell lines were all maintained in RPMI 1640 (Gibco) supplemented with 1% stable glutamine (PAA), 1% antibiotic-antimycotic (Gibco), 10% fetal bovine serum (FBS, Hyclone). Cells were kept in an incubator at 5% CO_2 at 37°C.

METHOD DETAILS

Isolation of human primary T cells

Human primary T cells were isolated from buffy coats obtained from healthy volunteers and in accordance with the recommendations of institutional guidelines (Radboudumc, Nijmegen, The Netherlands). All subjects gave written informed consent in accordance with the Declaration of Helsinki. Pan T cells were isolated from peripheral blood leukocytes using the Pan T cell isolation kit according to manufacturer's instructions (Miltenyi Biotec). Isolated human T cells were cultured in X-VIVO-15 medium (Lonza) supplemented with 2% human serum.

Isolation of murine primary T cells

Resting primary immune cells were isolated from either thymus, spleen or inguinal lymph nodes of WT and *Cd53*$^{-/-}$ mice (as indicated in figure legends). Organs were digested using collagenase type III (Worthington) and DNAse I (New England Biolabs) before being passed through a 100 μm filter. T cells were isolated using the Pan T Cell isolation kit II according to the manufacturer's instructions (Miltenyi Biotec). Cells were cultured in RPMI 1640 (Gibco) supplemented with 10% fetal bovine serum (FBS; Hyclone), 1% stable glutamine (PAA) and 1% antibiotic-antimycotic (Gibco), 1 mM sodium pyruvate (Gibco) and 0.1% 2-mercaptoethanol (Gibco). Isolated cells were used for experiments as described below.

T cell proliferation assays (human and murine)

One day prior to primary cell isolation flat-bottom high binding 96-well plates (Greiner Bio-one) were coated with indicated antibody combinations in 100 μL PBS and incubated overnight at 4°C. Plates were washed two times with PBS to eliminate unbound antibody before addition of cells. After isolation, cells were allowed to rest for 1 hour prior to staining with CellTrace Violet (CTV) (Thermo Fisher Scientific) in accordance with the manufacturer's instructions. After staining, cells were washed thoroughly with PBS before plating 1.5×10^5 cells to each well. Cells were then incubated for the indicated time at 37°C, 5% CO2, after which cells were stained for CD3, CD4 and CD8 and analyzed by flow cytometry (FACSVerse BD). FCS Express 6 software was used to analyze the proliferation of T cells based on CTV staining. The proliferation index is defined as the average number of proliferation cycles the cells have undergone in the indicated period of time. For human T cell activation, the following antibody concentrations were used for stimulation: 1 μg/mL anti-CD3, 5 μg/mL anti-CD28 and 5 μg/mL anti-CD53. For murine T cell activation, the following antibody concentrations were used for stimulation: 1 μg/mL anti-CD3 and 5 μg/mL anti-CD28.

IL-2 ELISA

IL-2 levels were measured using ELISA. These were performed on supernatants collected from stimulated primary T cells at the indicated time-points. The human IL-2 and murine IL-2 ELISA kits were used in accordance with manufacturer's instructions (Thermo Fisher Scientific).

KLH immunizations and ex-vivo recall assay

Eight-week-old female WT and *Cd53*$^{-/-}$ mice were immunized subcutaneously on day 0, 7 and 14 with NP-KLH (N-5060-5 Biosearch Technologies) or PBS as a control. Mice each received 100 μg NP-KLH adsorbed in alum (Sigma) on day 0, followed by subsequent

immunizations with 75 μg NP-KLH in alum per mouse on day 7 and 14. Spleens, inguinal lymph nodes and sera were harvested on day 21. Organs were processed as described in the above section, and T cells were isolated using the Pan T Cell isolation kit II according to the manufacturer's instructions (Miltenyi Biotec). Naïve antigen-presenting cells were isolated from an unimmunized (naïve) WT mouse by depleting T cells from the spleen using the CD3ε microbead kit according to the manufacturer's instructions (Miltenyi Biotec). T cells were stained with CTV as described in the above section and plated in 96-well flat-bottom plates at 1.5×10^5 T cells per well with/without 2×10^4 antigen-presenting cells isolated from naïve WT spleen. Cells were then stimulated with medium only (control) or 100 μg NP-KLH for 96 or 120 hours, after which cells were stained for CD3, CD4 and CD8 and analyzed by flow cytometry (FACSVerse BD). FCS Express 6 was used to analyze the proliferation of CD4+ T cells based on CTV staining and to determine the proliferation index as described above.

Differentiation of BMDCs from WT and *Cd53*$^{-/-}$ mice

Bone marrow cells were isolated and cultured in the presence of 200 ng/mL rFlt3L (eBioscience) in RPMI supplemented with 10% fetal bovine serum (FCS, Hyclone), 1% glutamine (Cambrex), 0.5% antibiotic/antimycotic (Invitrogen) and 50 mM beta-mercaptoethanol (Gibco) at 37°C, 10% CO2 for 9 days. Differentiated dendritic cells were analyzed for purity and composition by flow cytometry.

Assessing MHC-I and MHC-II expression on primary murine spleen-derived dendritic cells

Single cell suspensions of murine spleens were made by DNAse and collagenase treatment, after which DCs were enriched by Nycodenz density centrifugation as described in (Vremec et al., 2000). The plasma membrane of cells was stained with antibodies in PBS containing 1% BSA and 0.01% NaN3 (PBA) with 2% goat serum. Geometric mean fluorescence intensity was measured using flow cytometry.

In vitro antigen presentation assay

Spleens from OT-II mice were processed as described above and CD4+ positive T cells were obtained by using CD4+ isolation kit according to manufacturer's instructions (Miltenyi Biotec). After isolation, cells were stained with CTV in accordance with the manufacturer's instructions. BMDCs were incubated with 10, 50 or 100 μg/mL OVA (Endograde, Hyglos GmbH) or 1 μg/mL CD4 helper peptide (Anaspec) in complete RPMI-1640 for 1 hour (T helper peptide) or 6 hours (OVA protein) at 37°C. After incubation, cells were washed and incubated in complete RPMI-1640 containing OT-II CD4+ T cells (50000 cells/well) for 72 hours. FCS Express 6 was used to analyze the proliferation of CD4+ T cells based on CTV staining and to determine the proliferation index as described above.

In vivo antigen presentation assay

Spleens from OT-I mice were processed as described above and CD8+ positive T cells were obtained by using CD8+ isolation kit according to manufacturer's instructions (Miltenyi Biotec). After isolation, cells were stained with CTV in accordance with the manufacturer's instructions. 1×10^6 cells were injected intravenously in *Cd53*$^{-/-}$ and WT mice. The next day OVA immune complexes (OVA-IC) were injected intravenously and after 48 hours mice were sacrificed. Subsequently spleens were processed, and T cell proliferation was measured as described above. OVA-ICs were prepared by incubating different concentrations of soluble OVA (Endograde, Hyglos GmbH) with purified polyclonal rabbit IgG anti-OVA for 30 min at 37°C.

RMA-Muc1 tumor rejection model

Cd53$^{-/-}$ and WT mice were challenged subcutaneously with 5×10^6 RMA-Muc1 cells as described previously (Gartlan et al., 2013). Tumor growth was assessed by measuring bisecting diameters of each tumor with slide calipers two to three times a week. Tumor volume was calculated using the following published formula: 0.4(A × B2), in which A is the largest and B is the smallest dimension.

B16-OVA tumor cell immunization and ELISPOT

To measure T cell responses, mice were immunized intradermally at the base of the tail with 5×10^6 γ-irradiated B16-OVA melanoma cells in 100 μL of PBS. Antigen-specific T cell responses were determined by ELISPOT 14 days after immunization as previously described (Gartlan et al., 2013).

Cell labeling, immunoprecipitation, and mass spectrometry

For surface labeling, Raji and CEM cells were washed three times in Hank's buffered saline and incubated in PBS containing 0.5 mg/mL EZ-link-Sulpho-NHS-LC-biotin biotin (Thermo Fisher Scientific). After 30 min of incubation at 4°C, cells were washed three times in PBS to remove free biotin. Labeled cells were lysed at the concentration of 2×10^7/mL in lysis buffer containing 30 mM Tris, pH 7.4, 150 mM NaCl, 0.02% NaN3, protease inhibitors, 1% Brij97 (Sigma) and 1 mM EDTA. After 30 min at 4°C the insoluble material was removed by centrifugation at 12,000 g and the cell lysate was precleared by addition of heat-inactivated goat serum and protein G–Sepharose beads (GE Healthcare). Proteins were then immunoprecipitated by adding 1 μg mAb and 10 μL protein G–Sepharose beads to 200–400 μL of the lysate. After a 2-hour incubation at 4°C under constant agitation, the beads were washed five times in lysis buffer. The immunoprecipitates were separated by SDS/PAGE (5–15% gel) under non-reducing conditions and transferred to a PVDF membrane (Amersham Biosciences). Biotin-labeled surface proteins were revealed using Alexa Fluor

800-labeled streptavidin (Invitrogen). The data were acquired using the Odyssey Infrared Imaging System (LI-COR Biosciences). For mass spectrometry analysis, Raji cells were lysed in the above lysis buffer supplemented with 1 mM EDTA. The insoluble material was removed by centrifugation at 12,000 g for 15 min, before preclearing of the lysates using beads coupled to goat immunoglobulins. CD53 and CD81 were immunoprecipitated using Sepharose 4B beads coupled to the mAb TS53 or TS71. In order to identify and exclude from further analysis proteins that are not specifically co-immunoprecipitated with the target proteins, immunoprecipitation was similarly performed with an antibody to CD9 (TS9) that is not expressed by Raji cells. The proteins were separated by electrophoresis using 4-12% Tris-bis polyacrylamide gel (nupage, Invitrogen) under reducing conditions and stained with colloidal Coomassie Blue (imperial stain, Pierce). About 25 gel slices containing proteins were excised for each IP and destained in 200 μL 0,1 M NH4HCO3/acetonitrile v/v for 15 min, centrifuged and swollen in H2O repeatedly until completely destained. Gel pieces were then incubated in 150 μL 100% acetonitrile for 10 min and dried. This was followed by rehydration in 0,1 M NH4HCO3 containing 30 mg/mL TCEP (Tris(2-carboxyethyl) phosphine hydrochloride) for 10 min at room temperature. The TCEP solution was replaced with 55 mM iodoacetamide in 0,1 M NH4HCO3 for 30 min at room temperature in the dark. The gel pieces were washed in 150 μL 0,1 M NH4HCO3 for 10 min, before addition of 150 μL acetonitrile for 15 min, and then dehydrated in 100% acetonitrile, and dried. The gel pieces were then covered with a solution of trypsin (13.33 μg/mL in 0,1 M NH4HCO3) and incubated overnight at 37°C. After supernatant retrieval, the gel fragments were extracted twice by addition of 20 μL of Acetonitrile/5% formic acid (70/30 v/v) and incubated for 20 minutes at 37°C. Supernatants were pooled, dried, and rehydrated in Acetonitrile/formic acid/H_2O (3%/0.5%/96.5% v/v). LC-MS/MS analyses were performed using an ESI linear ion trap-Orbitrap hybrid mass spectrometer (LTQ-Orbitrap Velos, Thermo Fisher Scientific, Bremen, Germany) coupled in line with a nano-HPLC system (Ultimate 3000; Dionex) for liquid chromatography. 5 μL of digested protein was injected in the system by using a pre-concentration column (C18 trap column - PepMap C18, 300 μmID × 5 mm, 5 μm particle size and 100 Å pore size; Dionex). The nano-column used in this study was a PepMap C18 reverse phase (Acclaim pepmap RSLC 75 μm × 15 cm, nanoViper C18, 2 μm, 100 Å). A linear 45 min gradient (flow rate, 300 nL/min) from 4 to 55% acetonitrile in 0.1% (v/v) was applied. After the acquisition of a full MS scan by the Orbitrap at high resolution (30000 resolution, m/z range were 380–1700 Da) in the first scan event, the five most intense ions present were subsequently isolated for fragmentation (MS/MS scan). The collision energy for the MS/MS scan events was pre-set at a value of 35%, the isolation window was set at 3 Da, Dynamic exclusion option was enabled. The capillary voltage was set at 1.6 kV and the capillary temperature was 275°C. The data were analyzed using the Proteome Discoverer 1.4 software. The MS/MS spectra were searched against the Uniprot human Protein Database. The maximal allowed mass tolerance was set to 10 ppm for precursor ions and to 0.6 Da for fragmented ions. Peptide mass is searched between 350 Da and 5000 Da with time retention from 10 min to 50 min. Enzyme specificity was set to trypsin with a maximum of one missed cleavage. Carbamidomethylation of cysteine was set as a fixed modification. Protein N-terminal acetylation, oxidation of methionine, and carbamidomethylation of histidine, aspartic acid and glutamic acid were selected as variable modifications. Peptide identifications were validated by determination of false positives by Target decoy PSM validator. It is high if the false positive rate (FDR or false Discovery rate) is less than 1%, low if the FDR is greater than 5% and average (medium between 1 and 5%). Peptide identification Xcorr were calculated by the correlation of MS/MS experimental spectrum compared with the theoretical MS/MS spectrum generated by the Proteome Discoverer 1.4 software. A relative quantitation was performed with the Proteome Discoverer-integrated label free method which consists in comparing the mean peaks area of the three best peptides of a given protein. The method of calculation is three dimensional relying on retention time, ion intensity and m/z ratio of the peptide, with a mass error lower than 2 ppm. Proteins were considered only if they were identified with more than 2 peptides corresponding to only one protein (unique peptides), except for tetraspanins.

Immunoprecipitation and CD45 staining

Cells were lysed in a lysis buffer (30 mM Tris pH 7.4, 150 mM NaCl, protease inhibitors) supplemented with 1% Brij 97 and 1 mM EDTA. After 30 min incubation at 4°C, the insoluble material was removed by centrifugation at 10,000 x g and the cell lysate was precleared by addition of heat inactivated goat serum and protein G sepharose beads (GE Healthcare). Proteins were then immunoprecipitated by adding 2 μg mAb or 1 μL ascitic fluid and 20μL protein G-sepharose beads to 1 mL lysate. The immunoprecipitated proteins were separated by SDS-polyacrylamide gel electrophoresis and transferred to a PVDF membrane (GE Healthcare). For detection of CD45, the samples were reduced using beta-mercaptoethanol and CD45 was visualized using a combination of an anti-CD45 Rabbit mAb (D9M8I, from Cell Signalling ref #13917) and a dylight-800 labelled secondary antibody. For the detection of CD53 and CD81, the samples were kept unreduced and a combination of biotin-labelled antibodies (respectively TS53 and TS81: charrin et al., ref Eur. J. Immunol. 2003. 33: 2479–2489) and Alexa Fluor 680-labelled streptavidin was used. All acquisitions were performed using the Odyssey Infrared Imaging System (LI-COR Biosciences).

Proximity Ligation Assays

Proximity Ligation Assays (PLA) were performed using Duolink In Situ PLA Orange kit (Sigma-Aldrich), according to manufacturer's instructions. CEM T cells were fixed in 4% Paraformaldehyde (PFA) (Sigma), adhered on Poly-L-Lysine (PLL, Sigma-Aldrich)-coated cover glass slides (EMS Diasum), and probed with the indicated antibodies. Negative control PLA: anti-CD151 (11G5a) and anti-CD45 (ab10558); positive control PLA: anti-CD45 (MEM-28) and anti-CD45 (ab10558); CD53-CD45 PLA: anti-CD53 (MEM-53) and anti-CD45 (ab10558); Isotype control PLA: isotype control antibodies. All antibodies were used at 10 μg/mL. After performing the PLA, 4′,6-diamidino-2-phenylindole (DAPI) was used as nuclear stain and cells were embedded in Mowiol (Sigma). Cells were imaged

on a Zeiss LSM880 confocal microscope using the Airyscan Detector and a 63x oil immersion 1.4NA objective. The Zeiss Zen software was used to control the microscope to adjust spectral detection of the emission of DAPI and PLA-Orange (corresponding to Cyanine-3) and subsequent Airyscan Processing. Data was analyzed using Fiji image analysis software.

Micro-contact printing

CEM and Jurkat T cells were transiently transfected using the Neon transfection system ((Thermo Fisher Scientific) according to manufacturer's instruction, and cells were imaged 24 hours post-transfection with indicated expression constructs. Poly(dimethylsiloxane) stamps containing a regular pattern of circular spots with a diameter of 5 μm were prepared as described previously (van den Dries et al., 2012; Zuidscherwoude et al., 2017). Stamps were incubated for 1 hour with phosphate-buffered saline (PBS) containing anti-CD3 and anti-CD28 antibodies or isotype control antibodies (100 μg/mL) mixed with donkey anti-rabbit IgG (H&L)–Alexa Fluor 647 (10 μg/mL, Invitrogen) to visualize the spots. Stamps were washed with demineralized water and dried under a nitrogen stream. The stamp was applied to a cleaned glass coverslip for 20 seconds and then removed. Transfected cells were seeded on the stamped area and incubated at 37°C for 8 minutes. PFA was added to the cells to a final concentration of 2% PFA, or the coverslips were washed with PBS and fixed with 2% PFA in PBS for 20 min at room temperature. Samples were washed with PBS and demineralized water and embedded in Mowiol. Cells were imaged on an epifluorescence Leica DMI6000 microscope with a 63× oil 1.4 NA objective, a metal halide EL6000 lamp for excitation, a DFC365 FX CCD camera (Leica), and GFP, DsRed, and Y5 filter sets (for GFP, RFP, and Alexa Fluor 647, respectively; all from Leica). Focus was kept stable with the adaptive focus control from Leica. Data was analyzed using Fiji image analysis software.

Transfection and fluorescence lifetime imaging microscopy (FLIM)

Jurkat T cells were transiently transfected using the Neon transfection system according to manufacturer's instruction, and cells were imaged 24 hours post-transfection (Thermo Fisher Scientific). Phorbol 12-myristate 13-acetate (PMA) was used to induce the translocation of PKCθ to the plasma membrane. Live-cell microscopic analysis for FLIM in Jurkat T cells was performed on a SP8 confocal microscope equipped with a 60× water 1.2 NA objective (Leica) using appropriate laser lines and settings. FLIM images were recorded using the same setup with an excitation light at 495 nm provided by a pulsed white-light laser (Leica). Fluorescence (from 500 to 535 nm) was collected with an internal photomultiplier tube and processed by a PicoHarp 300 time-correlated single-photon counting system (PicoQuant). At least 50,000 photons were recorded for each individual cell. To obtain the fluorescence lifetimes, photon histograms containing all photons pooled for each individual cell were reconstructed from the photon traces with a custom programmed algorithm (C#.NET), and these histograms were fitted with single-exponential decay curves (OriginLab) to obtain donor fluorescence lifetimes. A biexponential fit was used to obtain the percentages of bound donor. The typical lifetime of the donor was a fixed fitting parameter in this analysis.

Generation of human polyclonal CD53-deficient CEM T cells by CRISPR/Cas9-mediated genome editing

One guide RNA pair targeting sequences TGATAGAGCCCATGCAGCCCAGG and GTGAGTCCTTACAGCAGATGTGG within the CD53 gene were designed using the Massachusetts Institute Technology CRISPR design tool and subcloned into the px335 Cas9 vector as described before (Hsu et al., 2013; Pyzocha et al., 2014). CEM T cells were seeded on day 0 at an optimal density of 3×10^5 cells/mL. On day 1 cells were transfected with 1 μg of each of the two guide RNA plasmids and 0.5 ug of pGFP2-C1 vector with a Neon Transfection System Kit and Neon Transfection System (Thermo Fisher Scientific) according to manufacturer's guidelines as described for this cell line. On day 3, CEM cells were selected by fluorescence-activated cell sorting based on GFP expression using FACS Aria III (BD Bioscience). Eight days later, CD53-negative CEM cells were selected by fluorescence-activated cell sorting using an A488-conjugated antibody against CD53 (MEM53, Novus Biologicals). CD53 deficiency was validated by flow cytometry and Western blotting.

FRAP of WT and *CD53*$^{-/-}$ CEM T cells

WT and *CD53*$^{-/-}$ CEM T cells were transfected using the Neon transfection system (Thermo Fisher Scientific) with 2 μg of plasmid encoding for human sGFP2-CD45RO or sGFP2-CD45RA. 24 hours post-transfection cells were seeded in Willco dishes and FRAP was performed using a Leica TCS SP8 SMD microscope equipped with a 60× water 1.2 NA objective (Leica) and an argon-ion laser set to bleach with 40% power at the 488 nm wavelength. We measured the fluorescence intensity in the bleach zone as well as the whole cell and background to correct for photobleaching and background signal. Immobile and mobile fractions were calculated manually and confirmed using the easyFRAP web tool (Koulouras et al., 2018). Fitting of the average curve was performed with OriginPro 8 (Originlab).

CD45 internalization assay

CD53$^{-/-}$ and WT CEM T cells were transfected using the Neon transfection system (Thermo Fisher Scientific) with 2 μg of plasmid encoding for human mCherry-CD45RO or mCherry-CD45RA. 24 hours post-transfection, cells were labeled with an anti-CD45RO or anti-CD45RA antibody and incubated at 37°C (5% CO2) for 0-, 3-, 6- and 24-hours post-labeling. Upon harvesting, cells were fixed in 4% PFA, and stained with a secondary Alexa-647 antibody to quantify the amount of CD45RO or CD45RA antibody remaining on the surface. Cells were then measured using flow cytometry (FACSVerse BD), and analysis was performed using the FlowJo software package.

Western blot CD45 isoform expression

5×10^6 WT and *CD53*$^{-/-}$ cells were harvested and lysed directly in 2x LaemmLi sample buffer (4% SDS, 20% glycerol, 0.004% bromophenol blue and 0.125 M Tris-HCl) supplemented with 10% 2-mercaptoethanol. Proteins were separated by SDS-PAGE and transferred to a polyvinylidene difluoride membrane (Millipore). Membranes were blocked with 5% BSA (Roche) in Tris-buffered saline and probed with specific antibodies, followed by a secondary staining with IRDye-conjugated antibodies. Bands were detected using the Odyssey infrared detector (LI-COR). Protein staining intensity was determined by Image Studio Lite software analysis.

Western blot CD45 dimerization

CD45 dimerization was detected by protein crosslinking (Xu and Weiss, 2002). For this CEM control and CD53−/− cells (5×10^6 cells) were washed twice with PBS and resuspended in 2 mM Sulfo-EGS (Thermofisher, cat#21566) and incubated for 1 hour at 4°C with end over end rotating. After incubation, the sulfo-EGS was quenched by adding Tris-HCl pH 7.6 (10 mM final concentration) and incubating on ice for 20 minutes. Next, the cells were washed twice with PBS and lysed in lysis buffer (10 mM Tris-HCl at pH 7.5, 150 mM NaCl, 1% NP-40, 1 mM EDTA supplemented with phosphatase and proteinase inhibitors). For Western blot analysis, samples were run on either 6% SDS-PAGE gels or NuPAGE 3 to 8% Tris-Acetate gels (Thermofisher, cat#EA0378BOX) and transfered to PVDF membrane. Blots were blocked with Li-Cor Intercept TBS blocking buffer (Li-Cor, cat#927-60001) and probed with anti-CD45 followed by detection with IRDye 800CW. Blots were scanned using a Typhoon Biomolecular Imager (Amersham). For quantification, the area above the uncrosslinked CD45 bands was quantified as a percentage of total CD45 (crosslinked and uncrosslinked bands) using Image Studio Lite 5.2.

Western blot for p-Tyr and pCD3 zeta (Y142)

For CEM T cells

Prior to the activation assay, WT and *CD53*$^{-/-}$ cells were incubated for 1 hour with RPMI without serum. For each timepoint 2×10^6 cells were incubated with mouse anti-CD3 antibody (OKT3, Bio X Cell, cat. no. BE0001-2) at a concentration of 1 μg/mL for 10 minutes on ice. After this incubation, cells were further incubated with goat anti-mouse antibody (Pierce. cat. no.31160) at a concentration of 5 μg/mL for 10 minutes on ice. Cells were transferred to 37°C and incubated for 2 or 5 minutes. Incubation was stopped by directly adding 5 mL of ice-cold PBS while transferring the cells to ice. After washing, the cells were lysed with lysis buffer containing 1% n-dodecyl-b-D-maltoside, 50 mM Tris [pH 7.5], 150 mM NaCl, 2 mM EDTA with Protease and phosphatase inhibitors. After incubation for 10 minutes on ice, the lysates were spun for 15 minutes at 10,000 rpm and the supernatant was collected for analysis by western.

For primary murine T cells

Mouse spleens were dissected from WT and *Cd53*$^{-/-}$ mice. Single cells were obtained by homogenization using a 100 μm cell strainer in PBS with 2 mM EDTA and 0.5% BSA. After homogenization, cells were counted, and T cells were isolated using a pan-T-cell isolation kit according to the kit protocol. After the isolation, cells were washed and incubated in RPMI without serum for 3 hours to let the cells rest. For each activation time point, 5×10^6 cells were collected, washed with ice-cold RPMI 1640 without serum and incubated with hamster anti-CD3 (clone 145-2C11, Invitrogen cat. no. 16-0031-82) and anti-CD28 (clone 37.51, Bio X Cell cat.no. BE0015-1) at a final concentration of 10 μg/mL for 10 minutes on ice. Antibodies were crosslinked using goat anti-hamster (Biolegend cat. no. 405501) by incubating at a final concentration of 10 μg/mL on ice for 10 minutes. Cells were transferred to 37°C and incubated for 2 or 5 minutes. Control cells were kept on ice. Incubation was stopped by directly adding 5 mL of ice-cold PBS while transferring the cells to ice. After washing, the cells were lysed with lysis buffer containing 1% n-dodecyl-b-D-maltoside, 50 mM Tris [pH 7.5], 150 mM NaCl, 2 mM EDTA with Protease and phosphatase inhibitors. After incubation for 10 minutes on ice, the lysates were spun for 15 minutes at 10,000 rpm and the supernatant was collected for analysis by western.

Both murine and CEM cells were then analyzed by western after separation on a 10% SDS-PAA gel. Membranes were blocked with Intercept TBS (Li-Cor, cat. no. 927-60001) for 1 hour at room temperature and incubated with different antibodies overnight at 4°C diluted in Intercept TBS. In case of the anti-tyrosine antibody 4G10, 0.1% Tween was included during the incubation. After extensive washing membranes were incubated with secondary antibodies and after washing scanned with Typhoon imager. Bands were quantified with Image Studio Lite 5.2 (Li-Cor).

Phospho-flow of CD3 zeta chains and Lck

T cells were isolated as described previously. Stimulation and fixation of cells were performed as previously described (Rip et al., 2020). Per well, 5×10^5 splenocytes were plated in 96-wells round-bottom plates at 4°C. Cells were subsequently washed with RPMI–5% FCS, followed by centrifugation at 400 g for 2 min at 4°C. The cells were stained with unlabeled anti-CD3/anti-CD28 (at concentration 10 μg/mL) in case of stimulated samples or RPMI-5 %FCS media in case of unstimulated samples for 30 min at 4°C. Samples were stained with the fixable live/dead viability (final dilution 1:1000) during the last 20 min of stimulation. The cells were subsequently washed and resuspended in RPMI-5% FCS media. The cells were stimulated by adding anti-armenian hamster IgG (at final concentration 10 μg/mL) to establish receptor crosslinking at 37°C for 5 min. In addition, anti-armenian hamster IgG only treated cells were included as control. When stimulation time was over, equal volume of fixation concentrate buffer (diluted 1 in 1 with the supplied Fixation and Permeabilization diluent; Invitrogen) was added and cells were incubated for 10 min at 37°C to fix the cells. After fixation, plates were spun down and subsequently washed twice using eBioscience Wash Buffer (diluted 1 in 10 in Milli-Q;

Invitrogen). Parallel to stimulated cells, 5 × 10^5 splenocytes per well were transferred to a 96-well round-bottom plate at 4°C. Samples were stained with the fixable live/dead viability stain (Invitrogen) for 20 min at 4°C and subsequently fixed with pre-diluted eBioscience fixation and permeabilization buffer (Invitrogen) for 10 min at 37°C. After fixation, plates were spun down and subsequently washed twice using pre diluted eBioscience Wash Buffer as described above. To proceed with flow cytometry procedures, fixed cell samples were stained intracellularly for cell surface markers such as CD4, CD8 and B220 in eBioscience Wash Buffer, in the presence of an FcR-blocking agent (Human TruStain FcX; BioLegend) to avoid nonspecific binding of the antibodies. The samples were incubated in the dark for 30 min at 4°C. Subsequently, plates were washed with eBioscience Wash Buffer, and samples were resuspended with either p-LCK (Y394), p-LCK (Y505) or pCD3z (Y142)-PE in eBioscience Wash Buffer and incubated for 30 min at room temperature in the dark. In case of p-LCK(Y394), an additional incubation step was included with a donkey anti-rabbit PE-conjugated Ab (Jackson ImmunoResearch) in eBioscience Wash Buffer for 15 min at room temperature in the dark. Upon completion of the staining, samples were washed and resuspended in MACS buffer (0.5% BSA and 2 mM EDTA in PBS) and measured using a flow cytometer (Lyric).

CD45 activity assay

Primary CD3+ T cells from the spleens of WT and *Cd53*$^{-/-}$ mice were isolated as described above. One day prior to cell isolation flat-bottom high binding 96-well plates (Greiner Bio-one) were coated with 1 μg/mL anti-CD3 and 5 μg/mL anti-CD28 in 100 μL PBS per well. Plates were incubated overnight at 4°C. Plates were washed two times with PBS to eliminate unbound antibody before addition of cells. After isolation, cells were allowed to rest for 1 hour, then washed thoroughly with PBS and resuspended in culture medium. T cells were then plated at concentration of 1.5 × 10^5 cells/well. Cells were then incubated for 24 hours at 37°C, 5% CO2. After incubation cells were collected and washed twice with phenol red free (PRF) RPMI 1640 (Gibco) supplemented with 0.5% FBS. Cells were equilibrated in PRF RPMI 1640 (Gibco) supplemented with 0.5% FBS for 15 minutes at 37°C, after which 0.5 μL of pCap-SP1 peptide (2 mM stock) was added to each well. The pCap-SP1 probe has been validated previously as a tool for the assessment of CD45 activity (Stanford et al., 2012; Szodoray et al., 2016). Cells were then incubated for 15 minutes at 37°C. Cells were then washed once in PBA supplemented with 10 mM Na3VO4, then washed twice more with PBA. CD45 activity, as indicated by geometric mean fluorescence intensity (gMFI) of the pCap-SP1 peptide, was measured by flow cytometry (FACSVerse BD). The pCap-SP1 gMFI of stimulated and unstimulated paired WT and *Cd53*$^{-/-}$ samples were used to define a CD45 activity fold change.

QUANTIFICATION AND STATISTICAL ANALYSIS

All statistical comparisons were made with GraphPad Prism 5 software, and data are expressed as mean ± SEM, SD, or 95% CI as indicated in the figure legends. Differences between means were analyzed with Student's t tests, Welch's t test, Mann-Whitney U test, one-way ANOVA, Kruskal-Wallis or two-way ANOVA as indicated in the legends. Statistical significance was set at $p < 0.05$.